DIGITAL ACCESS TO SCHOLARSHIP AT HARVARD
DASH.HARVARD.EDU

HARVARD LIBRARY

Molecular mechanisms of metabolic adaptation to endurance exercise

Link
http://nrs.harvard.edu/urn-3:HUL.InstRepos:39947172

Terms of use
This article was downloaded from Harvard University's DASH repository, and is made available under the terms and conditions applicable to Other Posted Material (LAA), as set forth at
https://harvardwiki.atlassian.net/wiki/external/NGY5NDE4ZjgzNTc5NDQzMGIzZWZhMGFlOWI2M2EwYTg

Accessibility
https://accessibility.huit.harvard.edu/digital-accessibility-policy

Share Your Story
The Harvard community has made this article openly available.
Please share how this access benefits you. Submit a story

Molecular mechanisms of metabolic adaptation to endurance exercise

A dissertation presented

by

Nelson Knudsen

to

The Committee on Higher Degrees in Biological Sciences in Public Health

in partial fulfillment of the requirements

for the degree of

Doctor of Philosophy

in the subject of

Biological Sciences in Public Health

Harvard University

Cambridge, Massachusetts

July 2018

©2018 Nelson Knudsen

All rights reserved.

Professor Chih-Hao Lee Nelson Knudsen

Molecular mechanisms of metabolic adaptation to endurance exercise

Abstract

Adaptation of cellular metabolism allows tissues to perform diverse, specialized functions. Endurance exercise training promotes aerobic oxidation of metabolic substrates in skeletal muscle by increasing mitochondrial capacity to utilize fatty acids supplied by lipolysis in white adipose tissue and spare stored glycogen. This metabolic fueling strategy sustains energy production during long bouts of exercise. In my thesis, I will outline how a cytokine produced locally by immune cells drives the conditioning of muscle and white adipose tissue to endurance exercise. The first study establishes that the metabolic adaptation of skeletal muscle to endurance exercise training is governed by the cytokine interleukin-13 (Il-13), which also mediates the metabolic benefits of endurance exercise training, including increasing muscle mitochondrial function and glucose tolerance. Il-13 activates signal transducer and activator of transcription 3 (Stat3) to increase transcription of a network of genes involved in fatty acid uptake and oxidation, mitochondrial respiration, and glycogen synthesis. In the second study, I demonstrate that in addition to its function in skeletal muscle, Il-13 acts as a critical regulator of beige adipose tissue development in response to β-adrenergic signaling. Lastly, I discuss two non-transcriptional mechanisms of Il-13 signaling that enhance mitochondrial oxidative metabolism in skeletal muscle. Collectively, my work highlights

the complex role of immune signaling in integrating tissue metabolism with the physiological demands of endurance exercise.

Table of Contents

Chapter 1. Introduction 1

Metabolic flexibility and energy metabolism 2

Physical activity and metabolic fitness 3

Metabolic adaptation of skeletal muscle to exercise training 3

Molecular mechanisms of skeletal muscle metabolic adaptation 4

Immune signaling in tissue homeostasis 7

Th2 signaling in metabolism 9

Preview of findings 10

Chapter 2. Type 2 immunity drives metabolic conditioning of muscle to endurance exercise 13

Abstract 14

Introduction 14

Results 15

Discussion 42

Materials and Methods 43

Chapter 3. Il-13 mediates beige fat biogenesis 61

Abstract 62

Introduction 62

Results 65

Discussion 78

Materials and Methods 81

Chapter 4. Discussion and Conclusion 87

Summary of findings 88

Non-genomic functions of Stat3 in Il-13 mediated exercise physiology 89

Il-13 signaling in protein translation 96

Discussion 100

Final remarks 102

References 103

Acknowledgments

This work would not be possible without the support and contributions of many people. Science is a team effort and I have been lucky to be surrounded by some of the best teammates from around the world. Specifically, I am grateful for the help and guidance of many members of the Lee Lab, past and present; Ryan Alexander, David Jacobi, Kris Stanya, Sihao Liu, Lynn Dai, Xiaobo Li, Justina Cho, Xiaohui Kong, Matt Gangl, Alec Hyde, Mayer Chalom, Mandy Liou, and Alex Yesian. I have also met some great friends and collaborators in other laboratories at Harvard throughout my studies and I would also like to thank them.

I would like to thank the faculty of my dissertation advisory committee Gökhan Hotamisligil, Robert Farese Jr., Amy Wagers, and James Mitchell for their years of help and guidance. Thank you also to the members of my preliminary qualifying exam committee, Gökhan Hotamisligil, Tiffany Horng and Laurie Goodyear. I am also very grateful for the support of Marianne Wessling-Resnick, who was the Biological Sciences in Public Health Program Director when I began my Ph.D. studies.

The support of my family and friends has been a constant source of strength for me throughout my education. They have always pushed me to do my best. I appreciate all of the sacrifices they have made to allow me to do what I love. I am especially thankful for my best friend and partner, Breezy, and our canine companion, Edison, for their ability to make everyday better and brighter.

Lastly, I would like to thank my advisor Chih-Hao Lee for his mentorship. Chih-Hao has an uncanny ability to push students to reach their potential as scientists and I feel very lucky to have been trained in his laboratory for the past several years.

Throughout my studies, Chih-Hao pointed me in the right direction when I was unsure of what to do next and challenged me to push the limits of what I though I could do. I will cherish his mentorship and friendship long after I have left his laboratory.

Chapter 1

Introduction

Metabolic flexibility and energy metabolism

Efficient allocation of energetic resources in the face of complex environmental challenges is key for survival. To meet these demands, the human body has developed mechanisms to promote systemic metabolic efficiency. In response to changes in energetic demands, metabolic resources are funneled towards key processes and away from those that are unnecessary. For example, during pathogen infection energy is rapidly used by bacterial killing monocytes and macrophages through glycolysis. In this case efficiency is less important because an effective inflammatory response must be generated for survival. The ability of metabolism to adapt and reprogram is also evident in normal physiology. Energy demands during feeding-fasting transitions rely on a glucose-fatty acid cycle (i.e., extra glucose is converted to stored fat at the fed state to be released and utilized at the fasted state). In the developing heart, energy substrate preference switches from glucose to fatty acid at birth. A similar switch can also be observed in prolonged physical activity. Evolution of many of these adaptive processes occurred when food availability was not constant, which is no longer the case in modern society. In light of this, the human body is maladapted for dealing with chronic over-nutrition. As a consequence, obesity has become a major health issue. Insulin resistance is among the metabolic diseases associated with obesity, in which the body loses the response to insulin in the control of the glucose-fatty acid cycle. There is an urgent need to understand pathways governing metabolic flexibility that will help the development of new and effective therapies to restore metabolic homeostasis.

Physical activity and metabolic fitness

Exercise reduces the risk of multiple diseases, notably the metabolic syndrome. Despite the known protective benefits, greater than 80% of adults in the US do not meet the current guideline for aerobic exercise (1-3 hours of moderate to vigorous exercise per week) [1]. In fact, over-nutrition and lack of physical activity are major contributors of the obesity epidemic. Physical activity was identified as one of five key lifestyle variables that reduced premature mortality including incidence of cancer and cardiovascular disease [2]. Although many focus on the goal of losing weight, many of the beneficial effects of exercise occur independently of body weight changes [1]. Therefore, understanding the molecular basis underlying metabolic adaptation to exercise may identify mediators of disease prevention.

Metabolic adaptation of skeletal muscle to exercise training

Aerobic/endurance exercise is an energy demanding process. In response to the increased metabolic activity of contracting skeletal muscle, the body elicits an integrated response involving multiple tissues and signaling/hormonal pathways to cope with increased energy and oxygen demands [3]. During exercise, increased heart and ventilation rates, along with catecholamine-stimulated hepatic glucose production, supply additional oxygen and metabolic substrates to the muscle [3]. As muscle glycogen depletion signals exhaustion [4], a coordinated effort to promote endurance is mediated by glycogen preservation mechanisms and by adrenergic signaling promoting lipolysis in adipose tissue to supply fatty acids for mitochondrial oxidation in muscle [4, 5]. This metabolic fueling strategy is met with specialized muscle fibers exhibiting

distinct energy substrate preferences and characteristics, typically identified by expression of motor protein isoforms and mitochondrial oxidative capacity. Oxidative muscle fibers (type I and type IIa) are highly enriched in mitochondria and the oxygen carrier myoglobin, allowing longer contraction before fatigue [5]. Glycolytic muscle fibers (type IId/x and type IIb) have distinct machinery for rapid and high strength contraction, but fatigue more quickly [5]. The composition of muscle fibers and metabolic substrate preference can be shifted by repeated bouts of exercise, or exercise training. Accordingly, with endurance training, mitochondrial respiratory capacity of skeletal muscle is enhanced through an increase in the number of oxidative muscle fibers and/or in the oxidative potential of all myofibers [5]. In contrast, resistance training causes muscle hypertrophy and a shift towards glycolytic metabolism [6].

Molecular mechanisms of skeletal muscle metabolic adaptation

Studies that first described increases in mitochondrial activity after exercise training were published over 50 years ago [7]. In the past two decades, several exercise-inducible transcription factors and co-regulators have been identified to mediate this process (Fig. 1.1). Notably, peroxisome proliferator-activated receptor gamma coactivator-1α (Pgc-1α) co-activates transcription factors, such as myocyte enhancer factor 2 (Mef2) and nuclear receptors, including peroxisome proliferator-activated receptor δ (Pparδ), estrogen related receptor α (Errα) and γ (Errγ), to control a network of genes involved in fatty acid oxidation and mitochondrial oxidative phosphorylation [8-11]. In contrast, co-repressors nuclear receptor co-repressor 1 (Ncor1) and silencing mediator for retinoid or thyroid-hormone receptors (Smrt)

suppress oxidative metabolism [12, 13]. Activation of intracellular signaling cascades such as calmodulin-dependent protein kinase II (CaMKII), sirtuin 1 (Sirt1), AMP activated protein kinase (AMPK), and mitogen activated protein kinase (MAPK) by calcium or energy flux during muscle contraction is believed to modify muscle metabolism in part, through crosstalk with transcription factors described above [5]. Transgenic manipulation or pharmacological activation of aforementioned factors in mice increases endurance capacity and prevents the development of obesity and metabolic disease, supporting the notion that these pathways can be therapeutically targeted even in the absence of physical activity [14-16]. Although these exercise-inducible factors are critical in regulating the metabolic adaptation to endurance exercise training, the upstream signals that activate them are still under investigation.

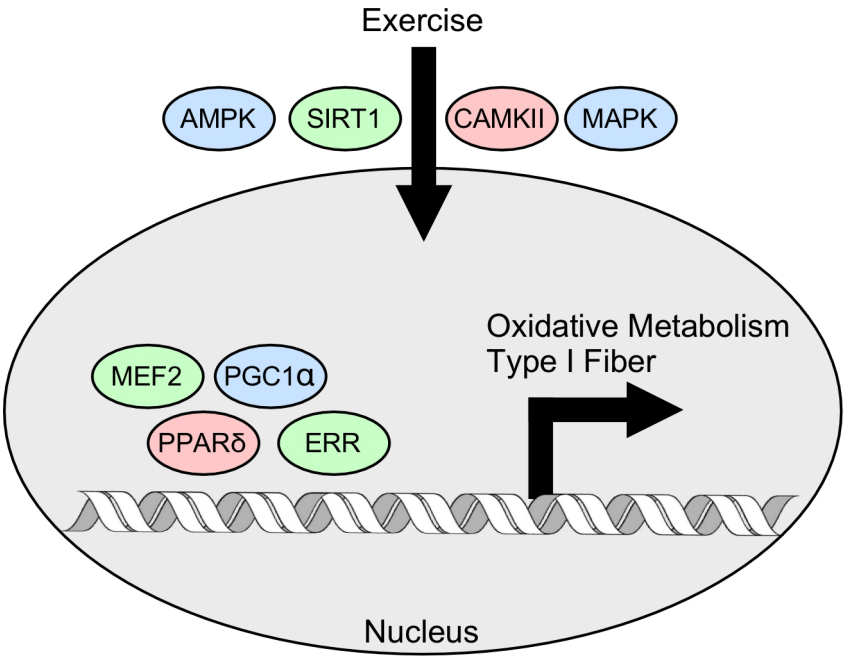

Figure 1.1. Molecular regulators of skeletal muscle oxidative metabolism. Exercise activates several signaling pathways that converge on transcriptional regulators of oxidative metabolism and muscle fiber type.

Immune signaling in tissue homeostasis

Resident immune cells serve critical functions in maintaining tissue homeostasis during acute and chronic stress. In addition to their role in mediating classical immune processes, such as pathogen infection, immune cells sense and adjust the metabolic set point of tissues by engaging both immune and metabolic signaling pathways [17]. During infection, inflammatory production of TNFα induces a transient insulin resistance to spare metabolic substrates for activated immune cells [18]. Production of classical inflammatory signals during chronic over-nutrition causes a state of metabolic inflammation or metaflammation, which further exacerbates insulin resistance and its associated pathologies [18]. Inflammatory activation and expansion of classically activated M1 macrophages in adipose tissue, liver and muscle contribute to the development of insulin resistance. Other innate and adaptive immune cell subsets have also been implicated in metabolic inflammation including $Cd4^+$ Th1 cells, $Cd8^+$ T cells and mast cells [19-21]. Conversely, there is a reduction in the abundance of inflammatory dampening M2 macrophages, regulatory T cells (T_{reg}), natural killer T (NKT) cells and invariant NKT cells [22-24]. These observations have led to a M1/M2 paradigm in that obesity shifts the immune set point towards a more inflammatory Th1 polarized immune state from a predominately Th2 polarized lean state (Figure 1.2).

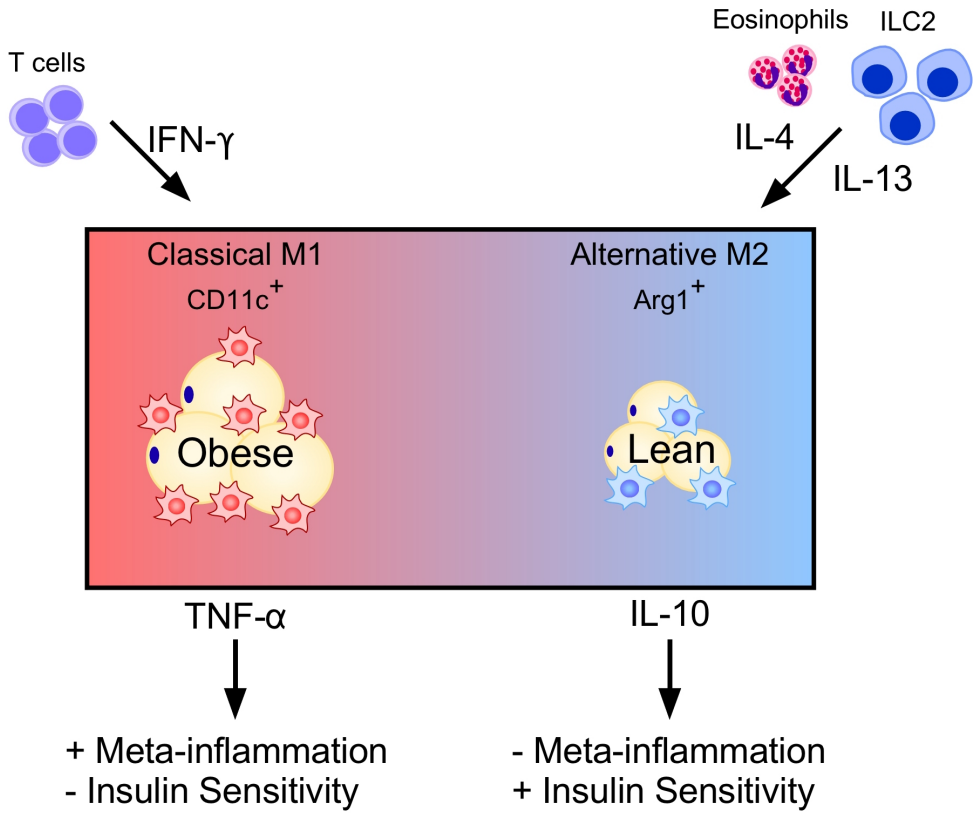

Figure 1.2. Integration of metabolic and immune signaling in adipose tissue (adapted from Knudsen and Lee, 2016 [25]). Obese adipose tissue is composed of adipocytes and CD11c^{+}, classical M1 activated macrophages that are polarized by T cell derived interferon γ (IFNγ). M1 macrophages in obese adipose tissue produce tumor necrosis factor α (TNF-α), which drives meta-inflammation and reduces insulin sensitivity. Healthy lean adipose tissue macrophages are polarized to an alternatively activated M2 state by eosinophil derived IL-4 and ILC2 derived IL-13. M2 macrophages produce IL-10 to dampen meta-inflammation and promote insulin sensitivity.

Th2 signaling in metabolism

As mentioned above, in the lean state, immune signaling is dominated by Th2 cytokine signaling which promotes insulin sensitivity and metabolic fitness [26]. The Th2 cytokines interleukin 4 (Il-4) and 13 (Il-13) have long-appreciated roles in Type 2 immunity, including the expulsion of helminth worms and responses to allergens [27]. Early studies showed that Th2 cytokines support white adipose tissue homeostasis by promoting alternative activation of resident macrophages through the canonical Th2 transcription factor signal transducer and activator of transcription 6 (Stat6) and its downstream effectors, Ppar and Ppar [28] [29]. In addition to more classical type 2 immune responses, Th2 cytokine signaling has been implicated in a variety of physiological processes [27]. During muscle regeneration, Il-4 signaling in fibroadipogenic progenitor stem cells (FAPs) through the canonical downstream effector Stat6 supports myogenic differentiation and repair [30]. Production of Il-13 by NKT cells in the liver directly acts on hepatocytes to suppress glucose production in response to feeding [31]. Il-13 action in hepatocytes is mediated by Stat3, and not Stat6, indicating a deviation in signaling between immune and non-immune cell types downstream of Il-13 [31].

Il-13 signals via the heterodimeric receptor of Il-13Rα1 and Il-4R, which it shares with Il-4 [32]. Il-4 is required for adaptive Th2 immunity as it utilizes an alternative receptor pairing consisting of Il-4R and the common gamma chain receptor (γ_c) that expresses in T lymphocytes. Il-13 is produced by a variety of innate and adaptive immune cells, notably type 2 innate lymphoid cells (ILC2) [27]. ILC2 were discovered as a peripherally distributed resident cell type that secretes Il-13 and Il-5 [33-35] and have

been associated with insulin sensitivity [36]. ILC2 and Th2 signaling have also been shown to regulate brown fat thermogenesis and beige cell recruitment [36-40]. The former has been challenged by a recent study [41]. Endurance exercise training also promotes the development of multilocular beige adipocytes in white adipose tissue [42]. It is currently unclear whether the ILC2-Th2 axis is involved in this process.

Preview of findings

In the chapters following I will discuss mechanisms of metabolic adaptation in two tissues in response to exercise (Figure 1.3). Chapter 2 examines the role of immune signaling in the metabolic adaptation of skeletal muscle to endurance exercise training. Specifically, we identified Il-13 as a critical regulator of muscle oxidative metabolism and mitochondrial biogenesis. Il-13 is produced in response to exercise training by muscle resident ILC2 cells and acts through the downstream transcription factor Stat3. This mechanism of metabolic adaptation promotes efficient use of metabolic substrates during exercise by promoting oxidative process such as fatty acid oxidation.

Chapter 3 is focused on the adaptation of adipose tissue to increased energy demand. We have examined the role of Il-13 signaling in adipose tissue beiging and thermogenesis. Il-13 signaling supports the development of beige adipose tissue, but is not required for normal thermogenic responses. Our studies indicate that beige adipose may serve additional functions other than heat generation in the context of endurance exercise, such as enhanced lipolysis.

In the final chapter I will discuss two additional mechanisms of Il-13 signaling in skeletal muscle that converge to enhance mitochondrial function. In addition to activating Stat3 transcriptional activity, Il-13 signaling promotes mitochondrial accumulation of Stat3 and its interaction with respiratory complexes and supercomplexes. Il-13 also appears to increase translation of nuclear-encoded mitochondrial transcripts by the ribosome. I will conclude the final chapter by discussing the overall significance of the work and some thoughts about future studies.

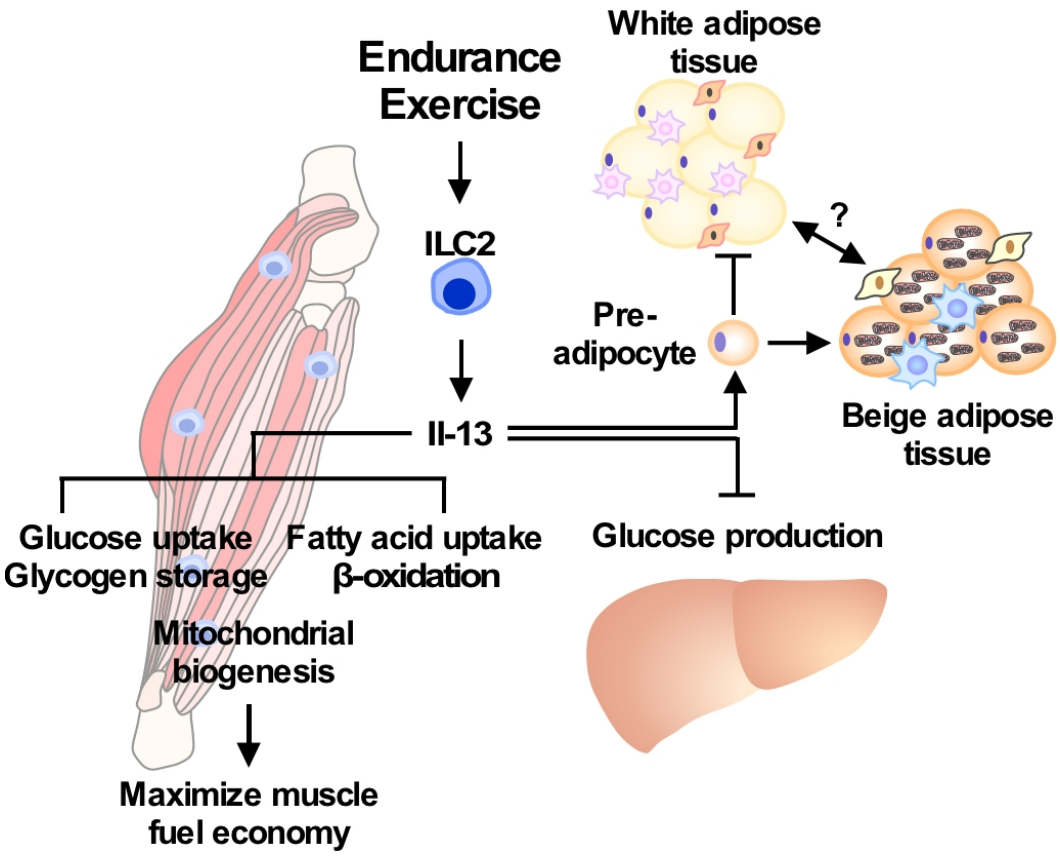

Figure 1.3. Metabolic adaptation to endurance exercise is coordinated by Il-13 signaling. Endurance exercise activates muscle resident ILC2 cells to produce Il-13, which increases muscle fatty acid oxidation and uptake, glycogen storage, and mitochondrial biogenesis. In addition, Il-13 signaling has been shown to promote the development of beige fat and limits white adipose tissue hypertrophy through regulation of pre-adipocytes and suppress glucose production from the liver.

Chapter 2

Type 2 immunity drives metabolic conditioning of muscle to endurance exercise

Nelson H. Knudsen, Kristopher J. Stanya, Alexander L. Hyde, Mayer M. Chalom, Ryan K. Alexander, Yae-Huei Liou, Matthew R. Gangl, David Jacobi, Sihao Liu, Vihang Narkar, Chad M. Paton, Jamie A. Cooper, and Chih-Hao Lee

(Submitted manuscript)

Abstract

Repeated bouts of exercise condition muscle mitochondria to meet increased energy demand, an adaptive response associated with improved metabolic fitness. We find Th2 cytokine interleukin-13 (Il-13) signaling is induced in endurance-trained muscle, where it orchestrates metabolic reprogramming that preserves glycogen store in favor of fatty acid oxidation and mitochondrial respiration. Il-13 acts through muscle Stat3 to up-regulate a transcriptional network involving estrogen-related receptors □/□. Accordingly, Il-13$^{-/-}$ mice have reduced running capacity and lost beneficial glycemia effects of exercise training, while enhanced muscle Il-13 signaling is sufficient to increase running distance, improve glucose tolerance and drive mitochondrial activity similar to that of endurance exercise. These results uncover coordinated immunological and physiological responses mediating exercise-elicited metabolic adaptations that maximize muscle fuel economy.

Introduction

Exercise reduces the risk of multiple diseases, notably the metabolic syndrome. Many of the beneficial effects of regular exercise occur independently of body weight changes [1]. Early studies have implicated unidentified humoral factors that mediate insulin-independent, exercise-induced muscle glucose uptake [43]. Subsequently, several “myokines” or muscle produced factors have been reported [44]. IL-6 is one of the first myokines described to be acutely induced after exercise. In vitro studies suggested that IL-6 enhances glucose utilization in differentiated myotubes [44]. However, resting IL-6 level is actually reduced by endurance training and increased in

obesity [44]. Il-6 gene deletion in mice also did not affect glucose uptake, substrate metabolism and running capacity; suggesting additional factors are involved in metabolic adaptation of prolonged physical activity [45, 46].

Results

To better understand the immunological response and identify circulating factors elicited by endurance exercise, we profiled a panel of human Th1/Th2 cytokines in serum from obese as well as normal weight sedentary and endurance-trained women (performing >1hr of aerobic exercise at least 4 times per week). Resting levels of IL-1β, IL-4, IL-10, and IFNγ were not altered among the groups (Fig. 2.1A and data not shown), while IL-6 and TNFα were elevated in obese female participants as reported. Endurance training increased the level of IL-13 but reduced IL-6 (Fig. 2.1A). Similarly, circulating Il-13 and Il-6 concentrations were higher and lower, respectively, in wild type (WT) mice subjected to 40 minutes of low intensity treadmill running for 5 days per week for 5 weeks, compared to untrained controls (Fig. 2.1B). Samples were collected 18 hours after the final bout of endurance exercise. These results indicate the immunological response to exercise is conserved between humans and mice. A primary source of Il-13 is tissue resident type 2 innate lymphoid (ILC2) cells [33]. In fact, ILC2 cells were identified as the major Il-13 producing cells in muscle (Fig. 2.1C and Fig. 2.2A-2.2D). Among Il-13^{+} cell populations, ILC2 cells were increased by exercise training (Fig. 2.1D), while T, natural killer (NK), and NKT cells remained unchanged (Fig. 2.2E). Furthermore, Il-13 gene expression was increased in whole muscle of exercise-trained mice, suggesting that local Il-13 signaling is elevated (Fig. 2.1E). To

examine the relevance of Il-13 in exercise physiology, we performed treadmill-running tests comparing WT and Il-13 whole body knockout ($IL13^{-/-}$) mice. $Il\text{-}13^{-/-}$ mice displayed a significant reduction in running time and distance (Fig. 2.1F). These results demonstrate that Il-13 is a candidate humoral factor induced by endurance training that modulates running capacity.

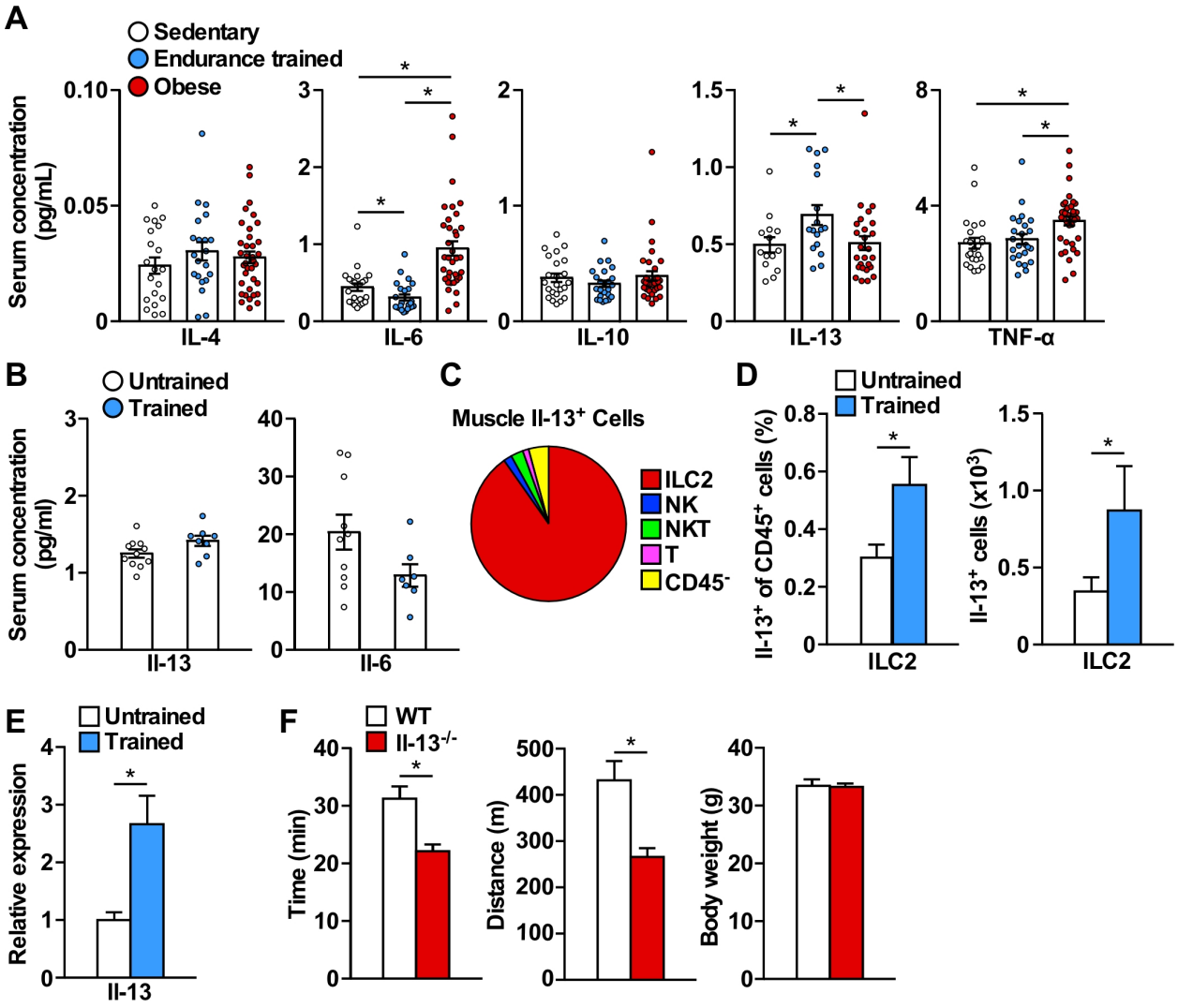

Figure 2.1. IL-13 is an exercise-inducible factor regulating endurance capacity (A) Resting human serum concentration of serum cytokines in normal weight sedentary control, endurance trained, and obese women. N=23-36/group, additional human cohort data included in Table 2.1, statistical analysis performed using Mann-Whitney test. (B) Resting serum concentration of Il-13 (p=0.053) and Il-6 (p=0.133) in untrained and endurance trained mice. N=7-12/group, 16 weeks old female mice, statistical analysis performed using Mann-Whitney test. (C) Il-13^{+} immune cell population in mouse skeletal muscle determined by flow cytometry. N=6, 16 weeks old male mice. (D) Quantification

(Figure 2.1 Continued) of skeletal muscle Il-13^{+} ILC2 cells in untrained and endurance trained mice as percentage (left panel) and total cell number (right panel). N=6/group, 16 weeks old male mice, statistical analysis performed using two-way ANOVA. (E) mRNA expression of Il-13 in gastrocnemius of untrained and endurance trained mice. N=5, 20 weeks old male mice, statistical analysis performed using unpaired Student's t test. (F) Endurance capacity test performed by treadmill running in WT and Il-13$^{-/-}$ mice. N=9/group, 15 weeks old male mice, statistical analysis performed using Mann-Whitney test. Additional mouse cohort data included in Table 2.2. Data presented as mean ± SEM. *$p<0.05$.

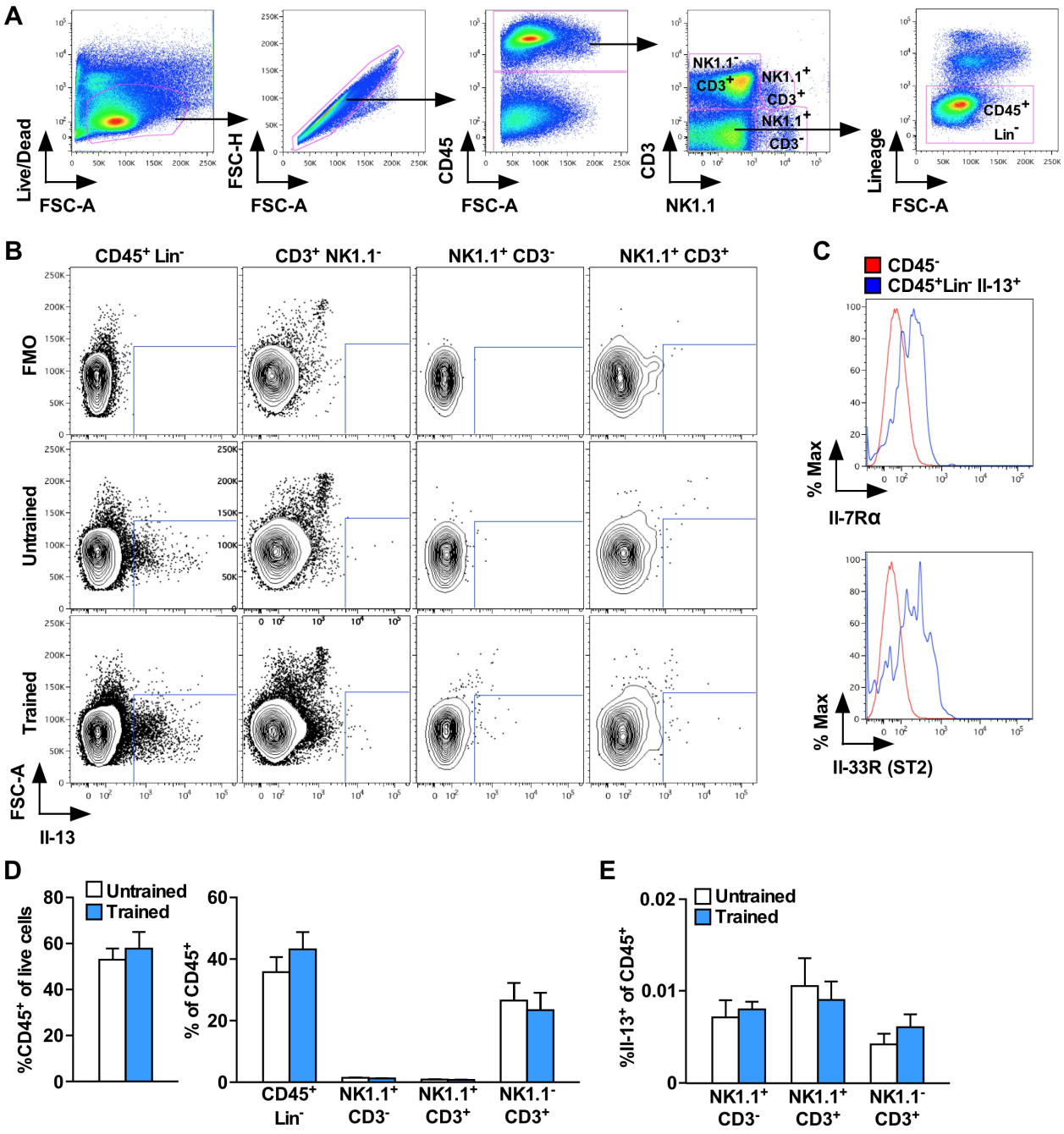

Figure 2.2. Assessment of Il-13-producing cells in skeletal muscle by flow cytometry. (A) Gating strategy for identification of Il-13^{+} cell population isolated from skeletal muscle. (B) Il-13 expression gating in various cell populations. FMO: fluorescence minus one, negative control. (C) Surface expression of additional ILC2

(Figure 2.2 Continued) markers Il-7Rα and Il-33R (ST2) in $CD45^{+}Lin^{-}Il\text{-}13^{+}$ versus $CD45^{-}$ cells. (D) Immune cell composition in untrained and endurance trained muscle. N=6, 16 weeks old male mice, statistical analysis performed using Mann-Whitney test (left panel) and two-way ANOVA (right panel). (E) $Il\text{-}13^{+}$ cell populations of NK ($NK1.1^{+}CD3^{-}$), NKT ($NK1.1^{+}CD3^{+}$), and T ($NK1.1^{-}CD3^{+}$) cells in muscle of untrained and endurance trained mice. N=6, 16 weeks old male mice, statistical analysis performed using two-way ANOVA. Data presented as mean ± SEM. *$p<0.05$

To determine the molecular basis of Il-13 signaling in regulating exercise physiology, we performed unbiased mRNA expression profiling by RNA-sequencing (RNA-seq) using gastrocnemius muscle samples from WT control and Il-13$^{-/-}$ mice with or without exercise training for 5 weeks as described earlier (Fig 2.3A). Gene ontology identified fatty acid metabolism and tricarboxylic acid (TCA) cycle as top biological processes up-regulated, comparing exercise trained versus sedentary WT mice (Fig. 2.4A). Among the genes up-regulated by exercise training were those involved in fatty acid uptake (e.g., lipoprotein lipase (Lpl) and acyl-coA synthetase long-chain family member 1 (Acsl1)), fatty acid beta-oxidation (e.g., carnitine palmitoyltransferase 1b (Cpt1b) and acyl-coA dehydrogenase very long chain (Acadvl)) and TCA cycle enzymes (e.g., pyruvate dehydrogenase alpha 1 (Pdha1) and isocitrate dehydrogenase 2 (Idh2)) (Fig. 2.3A and 2.4B). In addition, hexokinase 2 (Hk2), which is critical for exercise-stimulated muscle glucose uptake [47], glycogen branching enzyme (Gbe1) in glycogen synthesis and lactate dehydrogenase b (Ldhb), an enzyme converting lactate to pyruvate for entrance into the TCA cycle were also increased in exercised muscle. In contrast, glycogenolysis (e.g., phosphorylase kinase subunit gamma 1 (Phkg1)) was among the top biological processes down-regulated by endurance exercise in WT muscle (Fig. 2.3A and 2.4C-D). These data are in line with the notion that endurance training preserves muscle glycogen stores and promotes a metabolic switch from glycolysis to fatty acid oxidation [5]. However, this metabolic reprogramming was lost in Il-13$^{-/-}$ mice.

Consistent with the RNA-seq data, recombinant Il-13 (rIl-13) increased fatty acid uptake and β-oxidation and glucose uptake in differentiated C2C12 myotubes (Fig.

2.3B-C). Single bouts of acute exercise (30 min, 12 m/min) were used to examine the role of Il-13 in muscle substrate utilization *in vivo*. WT mice had significantly lower intramuscular triglyceride (TG, quadriceps) and maintained glycogen levels after exercise (Fig. 2.3D). Mice lacking Il-13 had reduced muscle glycogen content, while that of TG was unchanged. There was no difference in muscle TG and glycogen contents between WT and Il-13$^{-/-}$ mice at resting state. Serum lipid levels (TG and free fatty acid) were similarly elevated by exercise in both genotypes (Fig. 2.3E), suggesting that the exercise-elicited defect in Il-13$^{-/-}$ mice was muscle intrinsic and not at the substrate level. Using an enclosed metabolic treadmill chamber to measure VO_2 and VCO_2 during exercise, we determined that in WT mice, there was an initial increase, followed by a gradual decline in respiratory exchange ratio (RER, VCO_2/VO_2, Figure 2.3F), indicative of a switch from glucose to fatty acid oxidation as described in human studies [48]. RER in exercising Il-13$^{-/-}$ mice was higher throughout. Consistent with reduced running capacity (Fig. 2.1F), Il-13$^{-/-}$ mice also had lowered maximal oxygen consumption (VO_2max, Fig. 2.3G), a predictor of aerobic endurance [3]. Collectively, these data suggest that Il-13 regulates the metabolic substrates that fuel exercising muscle.

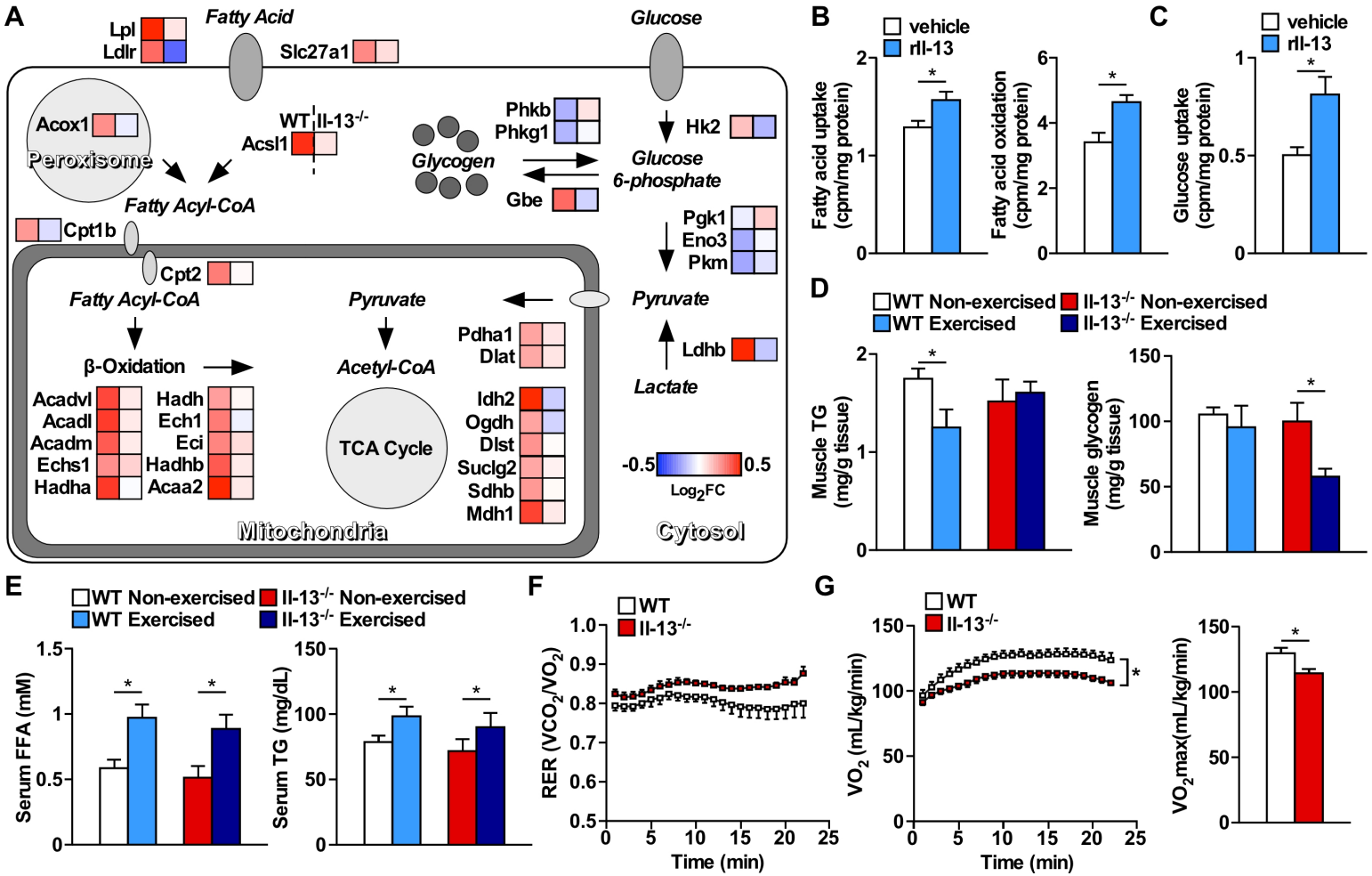
A
Fatty Acid
Glucose
Lpl
Ldlr
Slc27a1
Acox1
Peroxisome
WT
Il-13-/-
Acsl1
Glycogen
Phkb
Phkg1
Hk2
Glucose 6-phosphate
Gbe
Fatty Acyl-CoA
Cpt1b
Pgk1
Eno3
Pkm
Cpt2
Fatty Acyl-CoA
Pyruvate
Pyruvate
Pdha1
Dlat
β-Oxidation
Acetyl-CoA
Ldhb
Lactate
Acadvl
Acadl
Acadm
Echs1
Hadha
Hadh
Ech1
Eci
Hadhb
Acaa2
TCA Cycle
Idh2
Ogdh
Dlst
Suclg2
Sdhb
Mdh1
-0.5
0.5
Log2FC
Mitochondria
Cytosol
B
vehicle
rIl-13
Fatty acid uptake (cpm/mg protein)
Fatty acid oxidation (cpm/mg protein)
C
Glucose uptake (cpm/mg protein)
D
WT Non-exercised
WT Exercised
Il-13-/- Non-exercised
Il-13-/- Exercised
Muscle TG (mg/g tissue)
Muscle glycogen (mg/g tissue)
E
Serum FFA (mM)
Serum TG (mg/dL)
F
WT
Il-13-/-
RER (VCO2/VO2)
Time (min)
G
VO2 (mL/kg/min)
Time (min)
VO2max(mL/kg/min)

Figure 2.3. Il-13 regulates metabolic substrate utilization in exercising muscle. (A) Illustration of key metabolic genes in muscle metabolism regulated by endurance training in gastrocnemius of WT and Il-13$^{-/-}$ mice identified by RNA-seq. Data presented as heatmap (Log_2 Fold Change, trained versus untrained of the same genotype) with WT animals on the left and Il-13$^{-/-}$ on the right. Red indicates higher expression in exercised muscle, while blue indicates lower expression. N=4/group, 20 weeks old male mice. (B) Fatty acid uptake and oxidation in C2C12 myotubes treated with rIl-13 (10 ng/mL) overnight, statistical analysis performed using unpaired Student's t test. (C) Glucose uptake in C2C12 myotubes treated with rIl-13 (10 ng/mL) overnight, statistical analysis performed using unpaired Student's t test. (D) Triglyceride (TG) and glycogen content in quadriceps of control (non-exercised) and acutely exercised (single bout treadmill running), WT and Il-13$^{-/-}$ mice. N=4-5/group, 24 weeks old male mice, unpaired Student's t test. (E) Serum concentration of free fatty acids (FFA) and triglyceride (TG) in control and acutely exercised, WT and Il-13$^{-/-}$ mice. N=4-5/group, 24 weeks old male mice, statistical analysis performed using unpaired Student's t test. (F) Respiratory Exchange Ration (RER) of exercising WT and Il-13$^{-/-}$ mice. N=4/group, 24 weeks old female mice, statistical analysis performed using two-way ANOVA ($p=0.08$). (G) Respiration of exercising WT and Il-13$^{-/-}$ mice and quantification of maximal oxygen consumption (VO_2max). N=4/group, 24 weeks old female mice, statistical analysis performed using two-way ANOVA (left) and Mann-Whitney test (right). Data presented as mean ± SEM. *$p<0.05$.

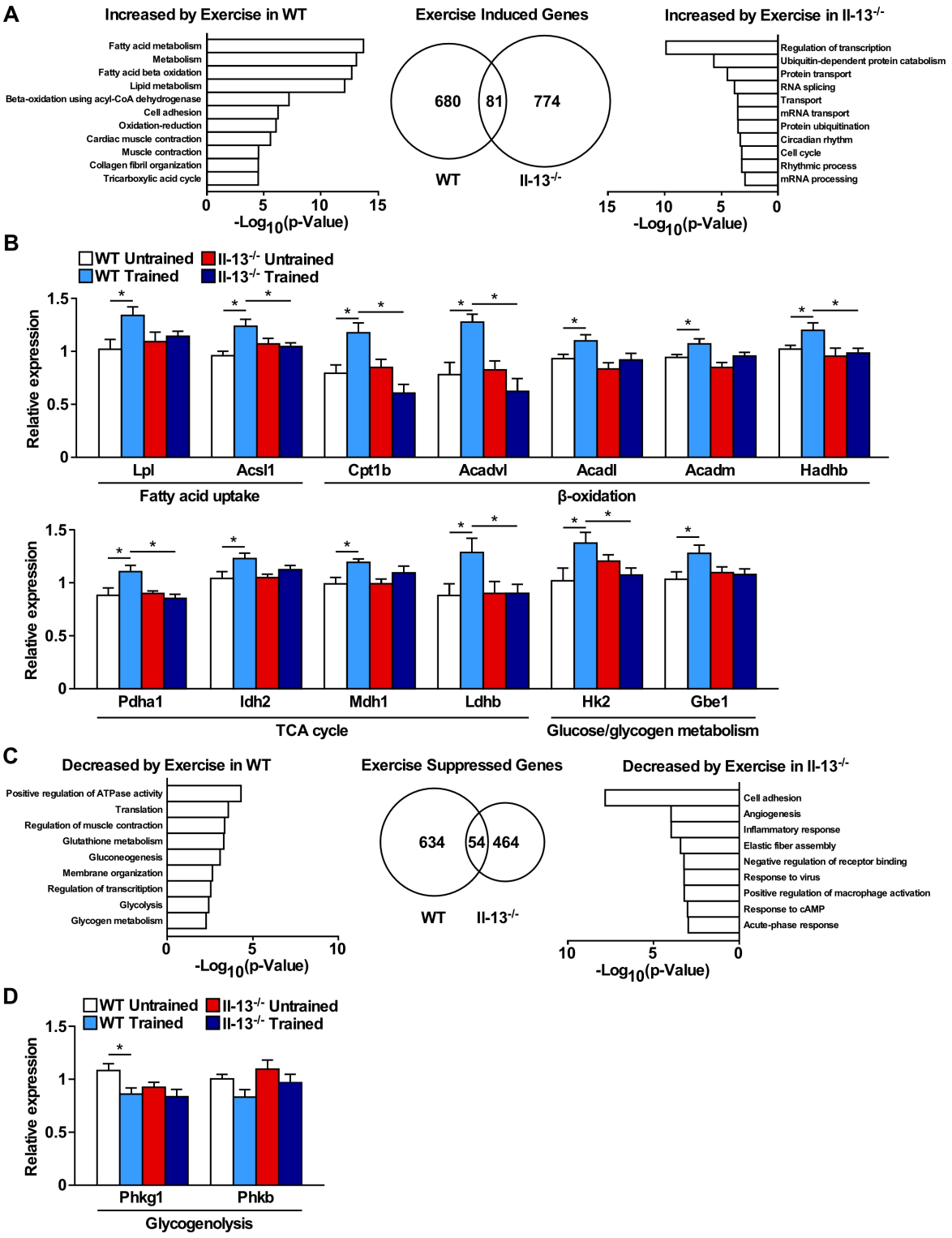

Figure 2.4. Muscle transcriptome analysis of exercise-trained versus untrained WT and Il-13$^{-/-}$ mice. (A) Enriched biological processes and Venn diagram of exercise

(Figure 2.4 Continued) induced genes in gastrocnemius of WT (left) and Il-13$^{-/-}$ (right) mice. (B) Validation of exercise-induced genes involved in fatty acid oxidation and TCA cycle in gastrocnemius of untrained and endurance trained, WT and Il-13$^{-/-}$ mice measured by qPCR. N=6-7/group, 20 weeks old male mice, statistical analysis performed using unpaired Student's t test. (C) Enriched biological processes and Venn diagram of exercise-suppressed genes in gastrocnemius of WT (left) and Il-13$^{-/-}$ (right) mice. (D) Validation of exercise-suppressed genes involved in glycogenolysis in gastrocnemius of untrained and endurance trained, WT and Il-13$^{-/-}$ mice measured by qPCR. N=6-7/group, 20 weeks old male mice, statistical analysis performed using unpaired Student's t test. Data presented as mean ± SEM. *$p<0.05$

Endurance exercise increases mitochondrial oxidative metabolism by increasing both mitochondrial biogenesis and respiratory capacity. Comparison of genes differentially regulated in muscle of WT and Il-13$^{-/-}$ mice further identified oxidation-reduction as a key biological process dysregulated in Il-13$^{-/-}$ muscle (Fig 2.5A), notably in the trained condition, in addition to fatty acid metabolism (Fig. 2.6A). Most genes in this category belonged to mitochondrial oxidative metabolism and were also increased by endurance exercise in WT mice (Fig. 2.5A and 2.6B). These included genes involved in the electron transfer flavoprotein, mitochondrial ribosome, mitochondrial protein import and components of electron transport chain (ETC) complexes. The expression of these genes was either unchanged or instead down-regulated by exercise training in Il-13$^{-/-}$ mice. In C2C12 myotubes, rIl-13 treatment led to higher basal and maximal mitochondrial oxygen consumption rate accompanied by an increase in mitochondrial biogenesis determined by mitochondrial DNA (mtDNA) to nuclear DNA ratio (Fig. 2.5B), while rIl-6 failed to promote respiration (Fig. 2.6C). Endurance training increased ETC complex proteins and numbers of oxidative fibers stained positive for succinate dehydrogenase activity (SDH^{+}) in WT gastrocnemius muscle, an effect lost in Il-13$^{-/-}$ mice (Fig. 2.5C-D). Along the same line, exercise training increased muscle mitochondrial respiration in an Il-13-dependent manner when given substrates for complexes II and IV, determined by Seahorse electron flow tests (Fig. 2.5E). Similar results were obtained for complex IV activity using a colorimetric assay measuring oxidation of cytochrome c (Fig. 2.5F). Muscle mitochondrial activity was similar between untrained WT and Il-13$^{-/-}$ mice (20 weeks old). Lastly, endurance training increased glucose tolerance in WT, but not Il-13$^{-/-}$ mice (Fig. 2.5G). Thus, while Il-13 signaling is

dispensable for basal mitochondrial respiration, it is necessary to increase muscle mitochondrial biogenesis and oxidative capacity and enhance systemic glucose homeostasis in response to exercise training.

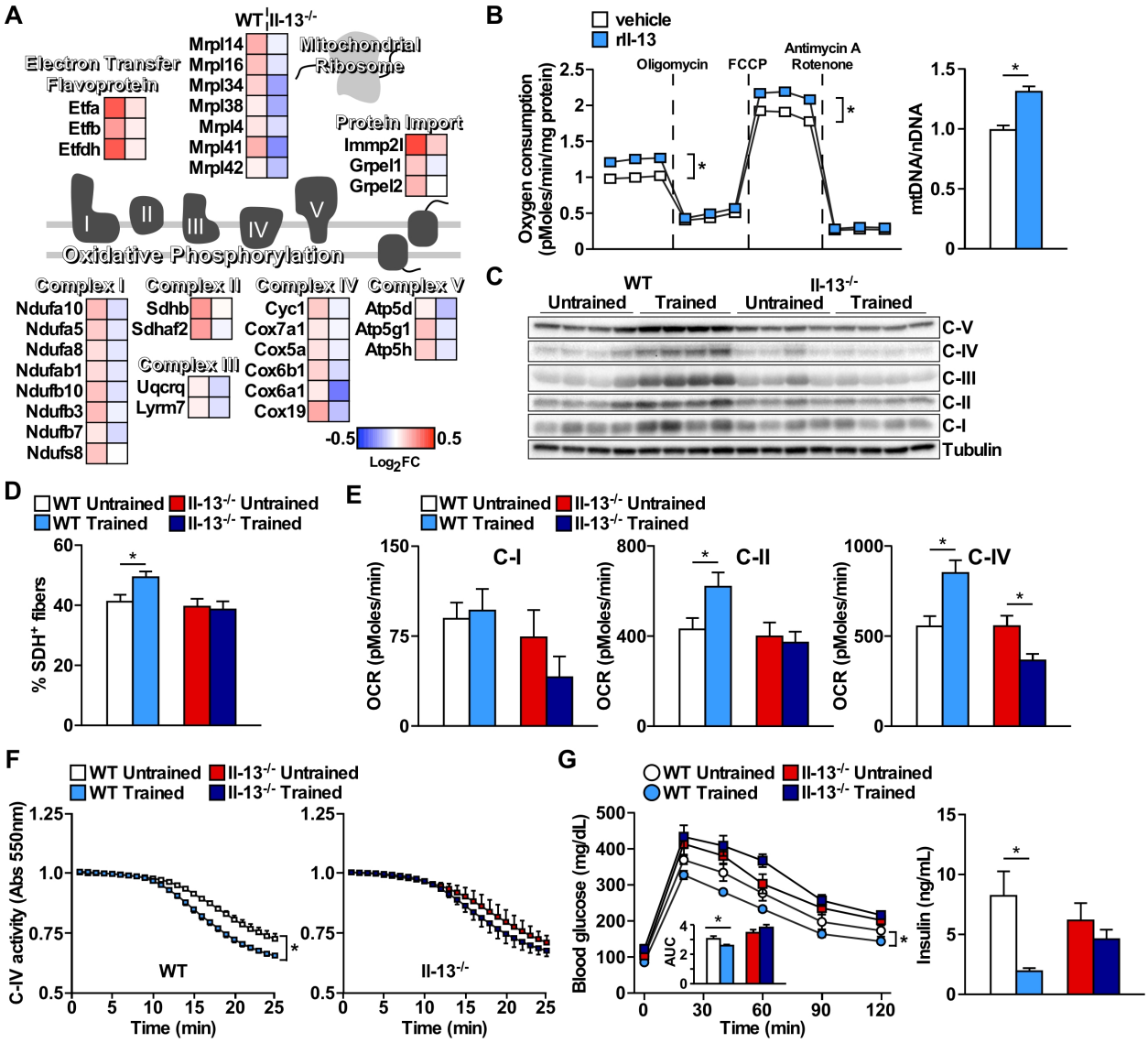

Figure 2.5. Mitochondrial biogenesis in endurance trained muscle requires Il-13 signaling. (A) Mitochondrial genes (representative) differentially regulated in gastrocnemius of endurance trained WT and Il-13$^{-/-}$ mice identified by RNA-seq. Data presented as heatmap (Log_2 Fold Change, trained versus untrained of the same genotype) with WT animals on the left and Il-13$^{-/-}$ on the right. Red indicates higher expression in exercised muscle, while blue indicates lower expression. N=4/group, 20 weeks old male mice. (B) Left panel: mitochondrial respiration of C2C12 myotubes

(Figure 2.5 Continued) treated with rIl-13 (10 ng/mL) overnight. Oligomycin was added to block ATP-coupled respiration, FCCP to induce maximal respiration, and antimycin A/rotenone to block mitochondrial electron transport. Right panel: mtDNA content of C2C12 myotubes treated with rIl-13 (10 ng/mL) overnight. Relative mitochondrial DNA content was measured by qPCR normalized to nuclear DNA, statistical analysis performed using unpaired Student's t test. (C) Western blot analyses of mitochondrial protein content of gastrocnemius from untrained and endurance trained, WT and Il-13$^{-/-}$ mice. N=4/group, 20 weeks old male mice. (D) Quantification of SDH^{+} muscle fibers in cross-sections of gastrocnemius from untrained and endurance trained, WT and Il-13$^{-/-}$ mice. N=4/group, 20 weeks old male mice, statistical analysis performed using Mann-Whitney test. (E) Electron flow assay using Seahorse bioanalyzer with mitochondria isolated from gastrocnemius of untrained and endurance trained, WT and Il-13$^{-/-}$ mice. Complex I (C-I) respiration was measured using pyruvate and malate as substrates and blocked with rotenone. Complex II (C-II) was measured using succinate as substrate and blocked with antimycin A. Complex IV (C-IV) respiration was measured by injecting TMPD/ascorbate. N=5-7/group, data combined from 3 experiments, statistical analysis performed using Mann-Whitney test. (F) Complex IV activity assay performed with mitochondria isolated from gastrocnemius of untrained and endurance trained, WT and Il-13$^{-/-}$ mice. The activity was assessed by the rate cytochrome c oxidation measured by the decline in reduced cytochrome c (absorbance at 550 nm). N=3-5/group, 20 weeks old female mice, statistical analysis performed using two-way ANOVA. (G) Left panel: glucose tolerance test (GTT) of untrained and endurance trained, WT and Il-13$^{-/-}$ mice. Inset: area under the curve (AUC). Right panel: fasting serum insulin levels of untrained

(Figure 2.5 Continued) and endurance trained, WT and Il-13$^{-/-}$ mice. N=5/group, 20 weeks old male mice, statistical analysis performed using two-way ANOVA for GTT and Mann-Whitney test for AUC and serum insulin. Data presented as mean ± SEM. *$p<0.05$.

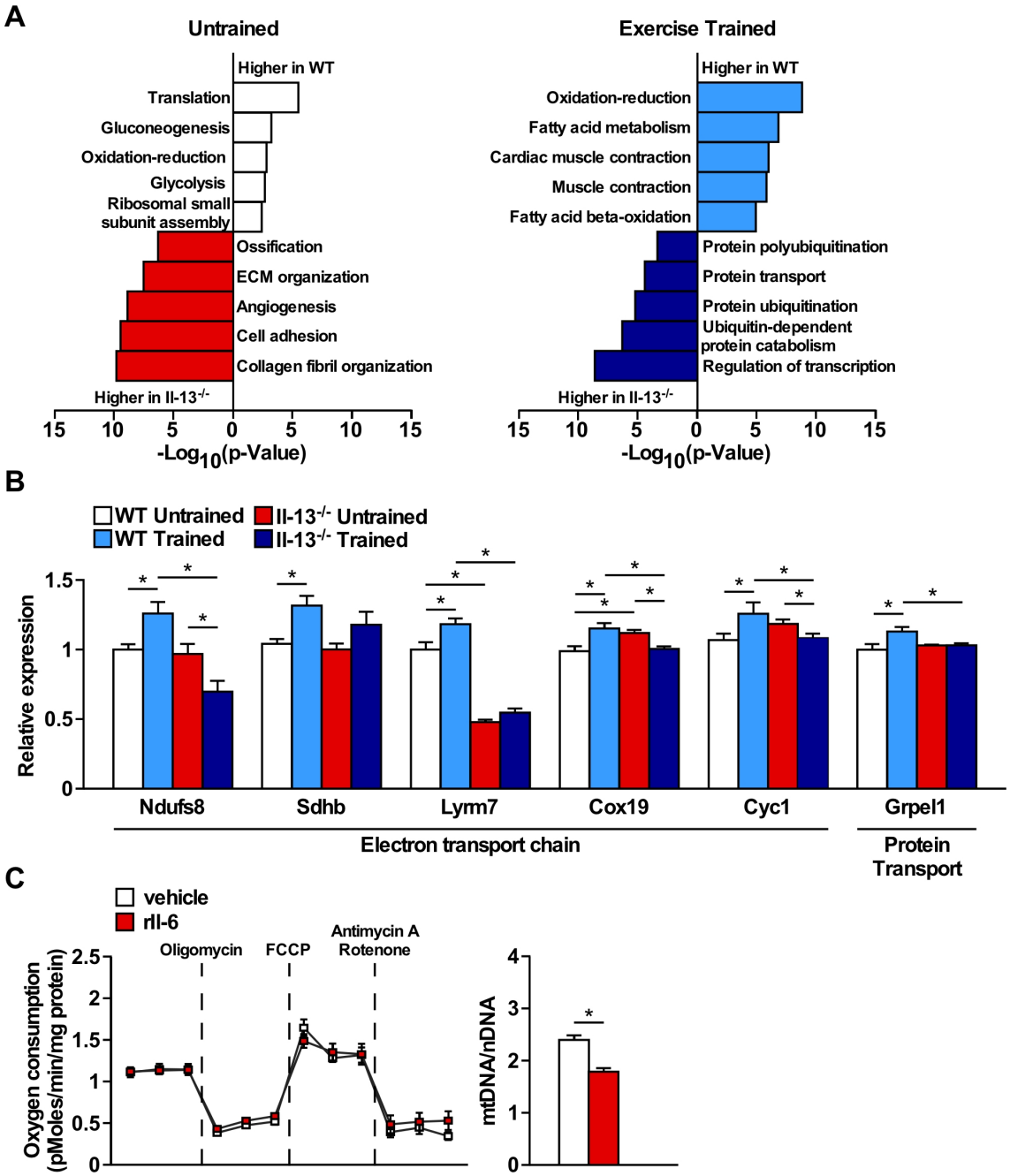

Figure 2.6. Muscle transcriptome analysis of WT versus Il-13$^{-/-}$ mice. (A) Enriched biological processes of differentially expressed genes in gastrocnemius of WT and Il-13$^{-/-}$ mice in the untrained (left) or endurance trained (right) state. (B) Validation of exercise-induced mitochondrial genes in gastrocnemius of untrained and endurance

(Figure 2.6 Continued) trained, WT and Il-13$^{-/-}$ mice measured by qPCR. N=6-7/group, 20 weeks old male mice, statistical analysis performed using unpaired Student's t test. (C) Left panel: mitochondrial respiration determined by seahorse mitochondrial stress test assay of C2C12 myotubes treated with rIl-6 (10 ng/mL) overnight. Right panel: mtDNA content of C2C12 myotubes treated with rIl-6 (10 ng/mL) overnight. Relative mitochondrial DNA content was measured by qPCR normalized to nuclear DNA, statistical analysis performed using unpaired Student's t test. Data presented as mean ± SEM. *$p<0.05$

Stat6 is the canonical transcription factor mediating transcriptional regulation by Th2 cytokines in immune cells. However, it is not expressed in muscle. *De novo* motif analysis of the promoters of mitochondrial genes differentially regulated in muscle of exercise trained WT and Il-13$^{-/-}$ mice identified several enriched binding sites for transcription factors, such as the Err nuclear receptors and Stat3 (Fig. 2.7A). Activation of Stat3 through Jak signaling downstream of Il-13Rα1 has been described in other cell types, including hepatocytes [31, 32]. In fact, Stat3 phosphorylation was elevated in muscle after either one bout of running or endurance training (Fig. 2.8A). Intramuscular injection of adenoviral Il-13 (adIl-13; adGFP was used as a control) into gastrocnemius muscle to increase local Il-13 levels (as it is secreted) induced Stat3 phosphorylation in quadriceps muscle (Fig. 2.7B and 2.8B). rIl-13 treatment in C2C12 myotubes also increased Stat3 phosphorylation (Fig. 2.8C), while stable knockdown of Stat3 abolished the ability of Il-13 to increase mitochondrial respiration, suggesting that Stat3 may be an effector of Il-13 in muscle. (Fig. 2.8D-E). Subsequently, skeletal muscle-specific Stat3 knockout (skmStat3$^{-/-}$) mice were generated by crossing Stat3$^{f/f}$ (control) to ACTA-1-cre mice (Fig. 2.8F). Similar to Il-13$^{-/-}$, skmStat3$^{-/-}$ mice run less on a treadmill, which was accompanied by reduced soleus muscle fatty acid β-oxidation (Fig. 2.8G). Elevated Il-13 signaling in muscle through gastrocnemius adIL-13 injection was sufficient to regulate the expression of exercise-controlled genes identified by RNA-seq (Fig. 2.7C), enhance respiration of isolated mitochondria from gastrocnemius given substrates for complexes II and IV (Fig. 2.7D), increase treadmill running time and distance (Fig. 2.7E) and improve glucose tolerance in control mice (Fig. 2.7F). These effects were completely abolished in skmStat3$^{-/-}$ mice. These observations indicate that Il-13 activates muscle

Stat3 to regulate mitochondrial oxidative metabolism during exercise. In addition, increasing Il-13 signaling locally in muscle drives an exercise-like effect on mitochondrial activity that is accompanied by increased running capacity and glucose tolerance.

The motif enrichment analysis indicated that the Err nuclear receptor family, known to be up-regulated by exercise [49] and control oxidative metabolism in both skeletal and cardiac muscle [11, 50], may be downstream of muscle Il-13-Stat3 signaling. In fact, RNA-seq data (validated by real-time PCR) demonstrated that exercise-induced muscle expression of Errα and Errγ was Il-13-dependent (Fig. 2.7G; Err expression was low). Furthermore, adIl-13 increased Errα and Errγ in quadriceps of Stat3$^{f/f}$ but not skmStat3$^{-/-}$ mice (Fig. 2.7H). Putative Stat3 binding sites were identified ~2kb upstream of the transcriptional initiation site for both Err and Err genes (Fig. 2.7I and 2.8H). Over-expression of Stat3 in AD293 cells was sufficient to increase the 2kb reporter activity of either Errα or Errγ in a dose-dependent manner, but not the 1kb promoter that lacked Stat3 binding sites. Mutation of the only Stat3 binding site in Errγ promoter abolished Stat3 regulation (Fig. 2.7I). To further examine the regulation in a relevant cell type, Stat3$^{-/-}$ C2C12 myoblasts were generated through CRISPR/Cas9. rIl-13 increased luciferase activity of the 2kb promoter in control but not Stat3$^{-/-}$ myoblasts (Fig. 2.7J and 2.8I). Reintroduction of Stat3 in Stat3$^{-/-}$ myoblasts increased basal promoter luciferase activities and restored the sensitivity to rIl-13 treatment. Collectively, these data implicate Il-13 as a regulator of the adaptive metabolic response of muscle to exercise training, in part, through a coordinated transcriptional program mediated by Stat3 and Errα/Errγ.

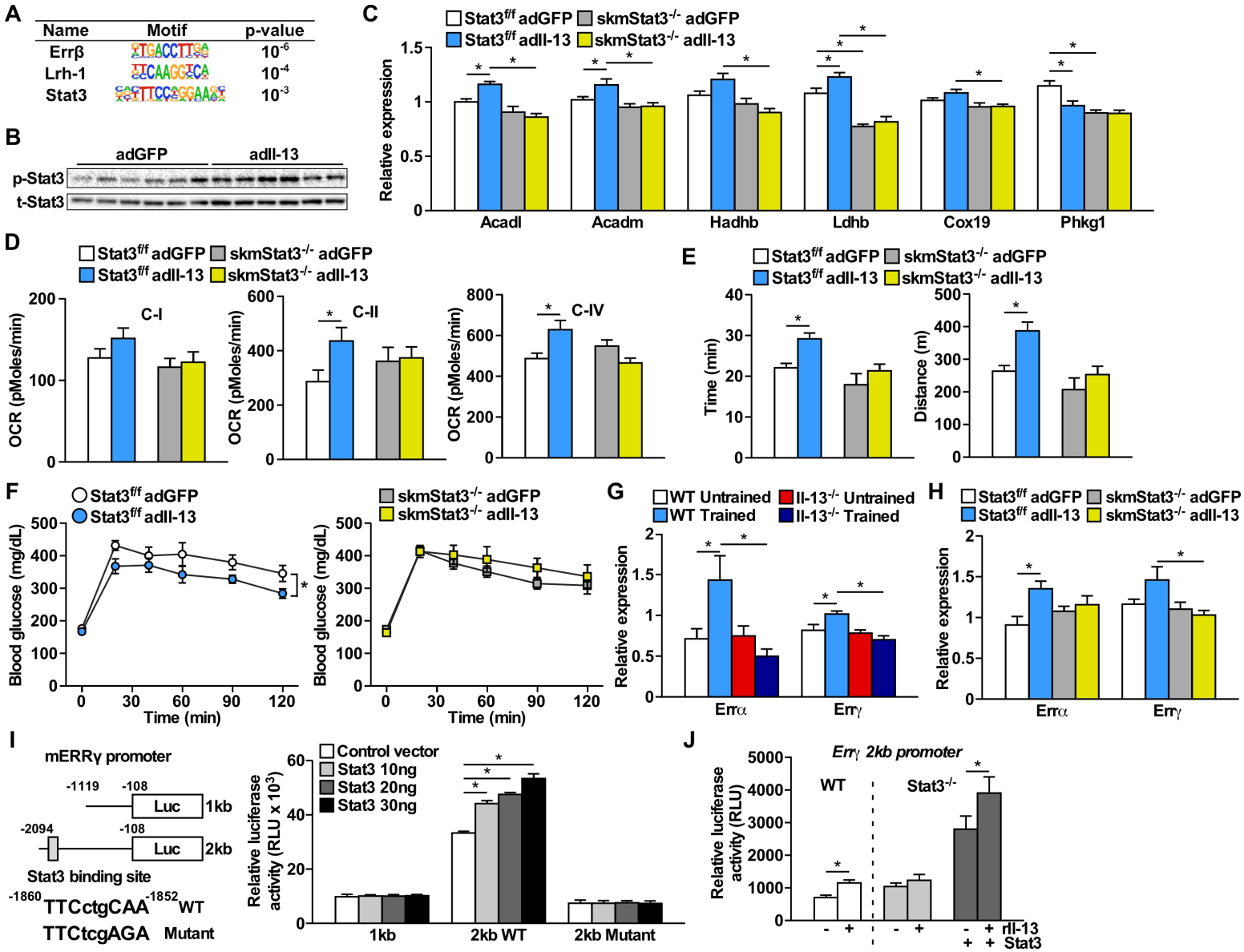
A
Name
Motif
p-value
Errβ
10-6
Lrh-1
10-4
Stat3
10-3
B
adGFP
adIl-13
p-Stat3
t-Stat3
C
Stat3f/f adGFP
skmStat3-/- adGFP
Stat3f/f adIl-13
skmStat3-/- adIl-13
Relative expression
Acadl
Acadm
Hadhb
Ldhb
Cox19
Phkg1
D
C-I
C-II
C-IV
OCR (pMoles/min)
E
Time (min)
Distance (m)
F
Blood glucose (mg/dL)
Time (min)
G
WT Untrained
WT Trained
Il-13-/- Untrained
Il-13-/- Trained
Errα
Errγ
H
I
mERRγ promoter
-1119
-108
Luc
1kb
-2094
2kb
Stat3 binding site
-1860 TTCctgCAA -1852 WT
TTCtcgAGA Mutant
Control vector
Stat3 10ng
Stat3 20ng
Stat3 30ng
Relative luciferase activity (RLU x 10³)
1kb
2kb WT
2kb Mutant
J
Errγ 2kb promoter
WT
Stat3-/-
Relative luciferase activity (RLU)
rIl-13
Stat3

Figure 2.7. Il-13 regulates muscle mitochondrial oxidative metabolism through Stat3. (A) *De Novo* motif analysis of promoters of Il-13 dependent, exercise-induced mitochondrial genes. (B) Western blot analyses of Stat3 phosphorylation (Y705) in quadriceps muscle of mice collected 7 days after injection of adGFP or adIl-13 into gastrocnemius muscle. N=6/group, 24 weeks old male mice. p-Stat3: phospho-Stat3; t-Stat3: total-Stat3. (C) mRNA expression of Il-13 dependent, exercise-induced genes in quadriceps muscle of $Stat3^{f/f}$ and $skmStat3^{-/-}$ mice collected 7 days after injection of adGFP or adIl-13 into gastrocnemius muscle measured by qPCR. N=6-8/group, 24 weeks old male mice, statistical analysis performed using unpaired Student's t test. (D) Electron flow assay performed with mitochondria isolated from gastrocnemius of mice described in C. Complex I (C-I) respiration was measured using pyruvate and malate as substrates and blocked with rotenone. C-II was measured using succinate as substrate and blocked with antimycin A. C-IV respiration was measured by injecting TMPD/ascorbate. N=4/group, 24 weeks old male mice, statistical analysis performed using Mann-Whitney test. (E) Endurance capacity test performed by treadmill running of $Stat3^{f/f}$ and $skmStat3^{-/-}$ mice 7 days after injection of adGFP or adIl-13 into gastrocnemius muscle. N=6-8/group, 24 weeks old male mice, statistical analysis performed using unpaired Mann-Whitney test. (F) Glucose tolerance test (GTT) of $Stat3^{f/f}$ and $skmStat3^{-/-}$ mice 6 days after gastrocnemius injection of adGFP or adIl-13. N=6-8/group, 24 weeks old male mice, statistical analysis performed using two-way ANOVA. (G) mRNA expression of Errα and Errγ in gastrocnemius muscle of endurance trained WT and $Il\text{-}13^{-/-}$ mice measured by qPCR. N=6-7/group, 20 weeks old males, statistical analysis performed using unpaired Student's t test. (H) mRNA expression of

(Figure 2.7 Continued) Errα and Errγ in quadriceps muscle of Stat3$^{f/f}$ and skmStat3$^{-/-}$ mice collected 7 days after gastrocnemius injection of adGFP or adIl-13 measured by qPCR. N=6-8/group, 24 weeks old males, statistical analysis performed using unpaired Student's t test. (I) Stat3 regulation of Errγ gene promoter in reporter transient transfection assays. Left Panel: Luciferase reporter constructs containing ~1kb and 2kb upstream of the transcriptional start site (TSS, designated as #1. Negative numbers indicate relative position upstream of TSS) of the Errγ gene. Putative Stat3 binding site and mutant binding site were indicated. Right panel: Relative luciferase activity of reporters in AD293 cells co-transfected with increasing amounts of Stat3 expression vector. Statistical analysis performed using two-way ANOVA. (J) Relative luciferase activity of 2kb Errγ promoter in WT and Stat3$^{-/-}$ C2C12 myoblasts. Stat3$^{-/-}$ Cells were co-transfected with a control or Stat3 expression vector ± rIl-13 overnight. Statistical analysis performed using unpaired Student's t test. Data presented as mean ± SEM. *$p<0.05$.

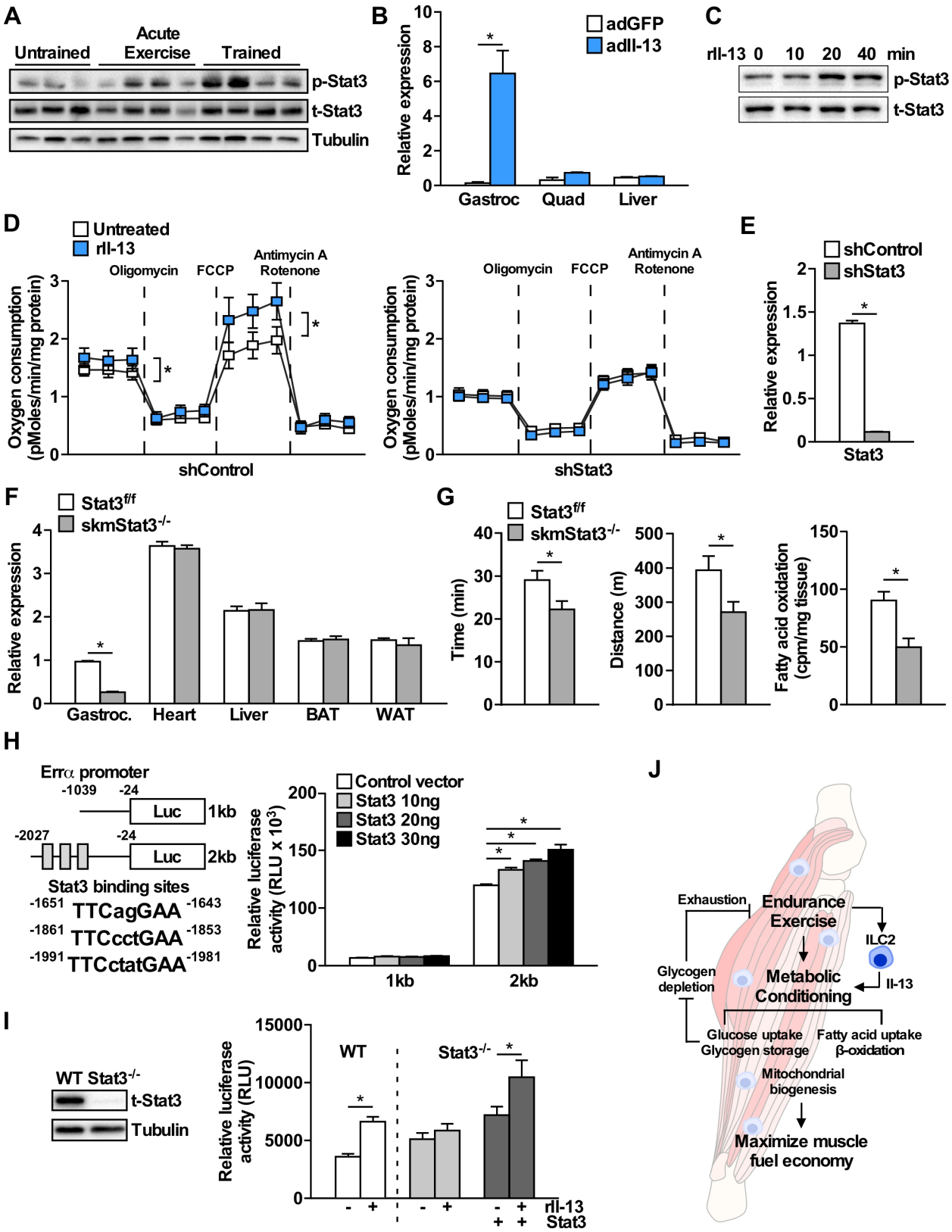
A
Untrained
Acute Exercise
Trained
p-Stat3
t-Stat3
Tubulin
B
adGFP
adIl-13
Relative expression
Gastroc
Quad
Liver
C
rIl-13 0 10 20 40 min
p-Stat3
t-Stat3
D
Untreated
rIl-13
Oligomycin
FCCP
Antimycin A
Rotenone
Oxygen consumption (pMoles/min/mg protein)
shControl
shStat3
E
shControl
shStat3
Relative expression
Stat3
F
Stat3f/f
skmStat3-/-
Relative expression
Gastroc.
Heart
Liver
BAT
WAT
G
Stat3f/f
skmStat3-/-
Time (min)
Distance (m)
Fatty acid oxidation (cpm/mg tissue)
H
Errα promoter
-1039
-24
Luc
1kb
-2027
-24
Luc
2kb
Stat3 binding sites
-1651 TTCagGAA -1643
-1861 TTCcctGAA -1853
-1991 TTCctatGAA -1981
Control vector
Stat3 10ng
Stat3 20ng
Stat3 30ng
Relative luciferase activity (RLU x 10³)
1kb
2kb
I
WT Stat3-/-
t-Stat3
Tubulin
WT
Stat3-/-
Relative luciferase activity (RLU)
rIl-13
Stat3
J
Exhaustion
Endurance Exercise
ILC2
Glycogen depletion
Metabolic Conditioning
Il-13
Glucose uptake
Glycogen storage
Fatty acid uptake
β-oxidation
Mitochondrial biogenesis
Maximize muscle fuel economy

Figure 2.8. Stat3 regulates mitochondrial respiration and running capacity downstream of IL-13. (A) Western blot analyses of Stat3 phosphorylation (Y705) in quadriceps muscle of untrained sedentary control, acutely exercised (30 min), and endurance trained (1 week) mice. N=3-4/group, 20 weeks old male mice. (B) mRNA expression of Il-13 in gastrocnemius (Gastroc), quadriceps (Quad), and liver of WT mice collected 7 days after injection of adGFP or adIl-13 into gastrocnemius muscle. N=2/group, 24 weeks old male mice, statistical analysis performed using unpaired Student's t test. (C) Western blot analyses of Stat3 phosphorylation (Y705) after acute treatment of C2C12 myotubes with rIl-13 (10 ng/mL). Samples were collected at indicated time points after rIl-13 treatment. (D) Mitochondrial respiration determined by seahorse mitochondrial stress test assay of shControl and shStat3 (shRNA knockdown) C2C12 myotubes treated with rIl-13 (10 ng/mL) overnight. Statistical analysis performed using unpaired Student's t test. (E) Knockdown efficiency of shStat3 in C2C12 myotubes measured by qPCR. Statistical analysis performed using unpaired Student's t test. (F) Deletion efficiency/specificity of Stat3 in various tissues of $Stat3^{f/f}$ and $skmStat3^{-/-}$ measured by qPCR. N=2/group, 24 weeks old male mice, statistical analysis performed using unpaired Student's t test. (G) Endurance capacity test performed by treadmill running and *ex vivo* fatty acid oxidation of isolated soleus muscle from $Stat3^{f/f}$ and $skmStat3^{-/-}$ mice. N=12/group, 24 weeks old male mice, statistical analysis performed using Mann-Whitney test. (H) Stat3 regulation of Err gene promoter in reporter transient transfection assays. Left Panel: luciferase reporter constructs containing ~1kb and 2kb upstream of the transcriptional start site (TSS, designated as #1. Negative numbers indicate relative position upstream of TSS) of the Errα gene.

(Figure 2.8 Continued) Putative Stat3 binding sites were indicated. Right panel: relative luciferase activity of reporters in AD293 cells co-transfected with increasing amounts of Stat3 expression vector. Statistical analysis performed using two-way ANOVA. (I) Left panel: western blot analyses of Stat3 protein expression in WT control and Stat3$^{-/-}$ C2C12 myotubes generated using LentiCRISPR v2. Right panel: relative luciferase activity of the 2kb Errα promoter in WT and Stat3$^{-/-}$ C2C12 myoblasts. Stat3$^{-/-}$ cells were co-transfected with a control or Stat3 expression vector ± rIl-13 overnight. Statistical analysis performed using unpaired Student's t test. (J) Endurance exercise activates Il-13 producing ILC2 cells in muscle to drive metabolic conditioning for maximal fuel economy. Metabolic conditioning promotes glucose uptake/glycogen storage, fatty acid uptake/oxidation, and mitochondrial biogenesis, leading to glycogen preservation that prevents exhaustion during exercise. Data presented as mean ± SEM. *$p<0.05$

Discussion

Metabolic conditioning of muscle to endurance exercise enhances fatty acid utilization and mitochondrial respiration, while reserving glycogen utilization, as a strategy to sustain energy supply for prolonged physical activity [4] (Fig. 2.8J). This coordinated effort extends metabolic flexibility/efficiency, which contributes to the beneficial effects of exercise on health. In the current study, we demonstrate the interplay between immune and metabolic pathways through Il-13 signaling in the control of energy substrate utilization in endurance exercise. Il-13 acts directly on muscle cells to increase fatty acid oxidation and mitochondrial ETC complex activity that is dependent on the downstream effector Stat3. Among the targets of the Il-13-Stat3 signaling are Errα and Errγ, two nuclear receptors also known to control fat catabolism and mitochondrial respiration in muscle [10, 11]. A previous study examining Err/Err cistromes in mitochondrial oxidative metabolism using ChIP-seq has predicted Stat3 binding sites co-localized with those occupied by Errs [51], implicating a feedforward mechanism for robust transcriptional outputs. Err/Err are “orphan” nuclear receptors without well-defined endogenous ligands [52]. How these receptors are activated remains unclear. Our results suggest that Il-13 may function as an upstream signal of the Stat3-Err transcriptional network.

Several lines of evidence indicate that IL-13 fits the criteria of a humoral factor mediating the metabolic benefits of exercise training. Endurance exercise leads to increased circulating IL-13 levels in mice and humans. Il-13 treatment increases the uptake of glucose and fatty acid in myotubes and exercise-induced mitochondrial biogenesis and glucose homeostasis require Il-13 signaling. Conversely, elevated Il-13

signaling in muscle drives exercise-like metabolic effects. Il-13 is not a classical myokine, since it is produced by ILC2 cells residing in muscle, where Il-13 is expected to be more concentrated. In this context, metabolic conditioning in endurance training resembles that of immunological memory in pathogen exposures. That is, repeated bouts of exercise trigger metabolic reprogramming and increase mitochondrial capacity building muscle "metabolic memory" to cope with increased energy demand. Interestingly, prior infection with helminth worm that elicits type 2 immunity in humans is associated with higher VO_2max [53], which has been used as an indicator of mitochondrial oxidative capacity and a predictor of running fitness. Il-13$^{-/-}$ mice have lower VO_2max compared to WT mice, consistent with reduced running time/distance and mitochondrial activity. These observations suggest that the coevolution of helminth worms and host may result in a beneficial effect of increased metabolic efficiency in the human hosts, perhaps in response to increased metabolic burden from the parasitic worms. Therefore, Il-13/Th2 signaling may have evolved to regulate metabolic adaptation to energy stress, such as in parasitic worm infection, endurance exercise, as well as previously reported cold-induced beige cell recruitment [37].

Materials and Methods

Animal studies

All animal studies were approved by the Harvard Medical Area Standing Committee on Animal Research. Mouse strains used in all experiments were in the C57Bl/6J background. Mouse genetic models were validated by both DNA genotyping and mRNA expression. Littermate controls were randomized to treatment groups based on body

weight and genotype. Animals are housed at 22° C in a barrier facility and kept on a 12 hr light, 12 hr dark cycle with free access to food and water. Experiments were performed in both sexes when possible. Detailed descriptions of all animal cohorts used for this study are included in Table 2.2.

Il-13$^{-/-}$ mice in the Balb/c background were obtained from Dr. A. McKenzie. Generation of Il-13$^{-/-}$ animals in the C57Bl/6J background was described previously [31]. These animals have been backcrossed >9 generations to C57Bl/6J mice from The Jackson Laboratory. Stat3$^{f/f}$ [54] animals were crossed to ACTA1-Cre mice (JAX#006149) from The Jackson Laboratory to generate skeletal muscle specific deletion of Stat3.

Human samples

Human serum samples were collected from obese, normal weight sedentary control and endurance athletes. Detailed descriptions of subjects are included in Table 2.1. Human studies were approved by the Institutional Review Board at Texas Tech University and informed consent was obtained prior to beginning any procedures.

C2C12 myoblast culture and cell line generation

C2C12 myoblasts were obtained from ATCC (CRL-1722). Myoblasts were maintained in culture at <80% confluence in DMEM (high glucose), 10% Fetal Bovine Serum (FBS). For differentiation, myoblasts were plated on collagen-coated plates. At confluence, media was changed from 10% FBS to 2% Horse Serum to induce differentiation. Myotube formation was monitored visually for 7-10 days prior to experimental use. For overnight treatment with rIl-13, myotubes were treated with 10 ng/mL rIl-13 (R&D

Systems, #413-ML) or vehicle control (0.1% BSA in PBS) in DMEM (high glucose) containing 2% Horse Serum for 18-24 hours. Acute signaling experiments were performed in myotubes after 1 hour incubation in serum free DMEM. rIl-13 was added at a final concentration of 10 ng/mL.

For generation of stable shRNA expressing cell lines, small hairpin target sequences were cloned into the pSIREN-RetroQ vector. The sequence for shRNA oligonucleotides can be found in Table 2.3. Retrovirus was produced by transfecting retroviral vectors into Phoenix packaging cells, followed by conditioned media collection. C2C12 myoblasts were incubated with retrovirus-containing conditioned media with 4 μg/mL polybrene and infected cells were selected with 2 μg/mL puromycin.

Stat3 knockout myoblasts were generated using LentiCRISPR v2 [55] containing a single gRNA for Stat3 from the mouse GeCKO v2 library [56]. The sequence for LentiCRISPR v2 Stat3 gRNA can be found in Table 2.3. Lentivirus was packaged in AD293 cells by transient transfection. Conditioned media containing lentivirus was used to infect C2C12 myoblasts. Cells were selected with puromycin and individual clones were characterized. Stat3 deletion was verified by western blot.

Primary myoblast isolation, culture, and differentiation

Primary myoblasts were isolated from mouse gastrocnemius, quadriceps, tibialis anterior and hamstring muscles. Muscle was excised and washed with cold PBS and placed in DMEM on ice. Samples were minced with scissors and transferred to 10 mL of 2 mg/mL collagenase (type II) and 0.5 mg/mL dispase in DMEM at 37°C with shaking for 1 hr. The cell suspension was dispersed 20 times with a 10mL pipette and

centrifuged at 50g to spin down large muscle pieces. The supernatant was passed through a 70μm cell strainer and centrifuged at 500g. The cell pellet was washed twice, re-suspended in Ham's F10, 20% FBS with 10 ng/mL bFGF and plated on collagen-coated culture dishes. Fresh media and bFGF were added every other day while cells were expanded for 8 days. Cells were then plated for differentiation in collagen-coated culture plates. Media was changed to 4% horse serum in Ham's F10 without bFGF to induce differentiation. Cells were differentiated for 8-10 days prior to experiments. For overnight treatment with rIl-13, primary myotubes were treated with 10 ng/mL rIl-13 or vehicle control (0.1% BSA in PBS) in Ham's F10 media containing 4% Horse Serum for 18-24 hours.

AD293 culture and transfection

AD293 cells were used for transcriptional reporter assays. Cells were maintained in 10% FBS in DMEM (high glucose).

Endurance running capacity test

Mice were acclimatized to the treadmill for 3 consecutive days at low speed (5 m/min) with no incline for 5 minutes. Running tests were performed with 5° incline. Animals ran at 10 m/min for the first 10 minutes followed by increases of 2 m/min every 5 minutes until exhaustion, which was defined by inability to remain on the treadmill for >5 seconds. Animals were removed immediately following exhaustion. An Exer-3/6 treadmill from Columbus Instruments was used for all treadmill running tests.

Endurance exercise training

Mice were acclimatized to treadmill running as outlined above before endurance exercise training. Endurance training was performed as described previously with minor changes detailed below [15]. Animals performed a single bout of running 5 days/week for the duration of exercise training (see detailed list of animal cohorts). All bouts of exercise were performed at the start of the dark cycle (ZT10-ZT14) to minimize disruption to the circadian rhythm. Animals ran 12 m/min for 30 minutes per day with 5° incline for the first week of exercise training, followed by an increase to 40 minutes per day in the second and subsequent weeks. Animals from both genotypes were able to perform all bouts of exercise. We did not observe changes in body weight or food intake in animals performing up to 6 weeks of exercise training.

Tissues and serum from endurance exercise trained mice were collected 18-24 hours after the final bout of exercise to limit acute effects of exercise.

Acute exercise

Mice were acclimatized to treadmill running as outlined above. Animals were fasted for 4 hours prior to single bouts of acute exercise set for 30 minutes at 12 m/min with 5° incline. Tissues and serum were harvested immediately following the single bout exercise.

Respirometry during exercise

Respiration during exercise was measured using a Metabolic Modular Treadmill connected to an Oxy-Max Comprehensive Lab Animal Monitoring System from

Columbus Instruments. Mice were acclimatized to treadmill running and fasted for 4 hours prior to measurements. A single animal was placed in the chamber followed by a baseline respiratory measurement for 5 minutes. The animal then performed an endurance running test starting at 10 m/min for 10 minutes with subsequent increases of 2 m/min every 5 minutes until exhaustion. Exhaustion was determined by inability to remain on the treadmill for >5 seconds or a rapid increase in RER.

Intramuscular injection of adenovirus

Virus was administered by direct injection into gastrocnemius as described by others [57]. Animals were anesthetized with isoflurane inhalation. Each muscle received 50 μL of 10^{10} PFU/mL adGFP (control) or adIL-13 virus. Animals were allowed to recover for 72 hrs before any experimental procedures were performed. Mitochondria were isolated from gastrocnemius muscle. Protein and RNA were isolated for western blot and gene expression studies from quadriceps.

Glucose tolerance

Mice were fasted overnight prior to glucose tolerance test. Fasting blood glucose was measured and animals were injected with glucose at 1.5 g/kg body weight into the peritoneum. Blood glucose was measured at 20, 40, 60, 90 and 120 minutes post injection. Animals performed the previous bout of exercise at least 12 hours prior to start of glucose tolerance test to avoid acute effects of exercise on glucose metabolism.

Cell isolation and flow cytometry

Single cells were isolated from gastrocnemius, quadriceps, tibialis anterior and hamstrings. Muscles were minced and digested with 0.4 units/mL Liberase TM, 0.1 mg/mL DNase I, 10% FBS in DMEM for 45 minutes. The cell suspension was centrifuged at 500g for 5 minutes and the pellet was incubated for another 45 minutes in fresh digestion buffer. The cell suspension was passed twenty times through a 10 mL pipet to release cells, centrifuged at 50g for 5 minutes to remove large debris and passed through a 70 μm cell strainer. Cells were washed with 10% FBS DMEM and overlaid onto 40% percoll for centrifugation at 500g for 20 minutes. Pelleted cells were washed with PBS and red blood cells were lysed before counting. For each animal, 1 million cells were used for staining for FACS analysis. Cells were blocked with TruStain FcX (Biolegend, #101320) and stained with Fixable Viability Dye eFluor 455UV (eBioscience, #65086818). Extracellular markers were stained with BV650 anti-mouse CD45 (Biolegend #103151), FITC anti-mouse Lineage Cocktail (Biolegend #78022), PerCP/Cy5.5 anti-mouse CD127(Il-7Rα) (Biolegend #121113), PE-Cy7 anti-mouse CD3 (eBioscience #25003182), APC anti-mouse Il-33Rα (Biolegend #145306), and APC/Cy7 anti-mouse NK1.1 (Biolegend #108723). Cells were then fixed and permeabilized with the Intracellular Fixation and Permeabilization Buffer Set (eBioscience, #88882400). Intracellular staining for Il-13 was performed with PE anti-mouse Il-13 (eBioscience #12713381). Staining was analyzed on a BD LSRFortessa Cell Analyzer.

Serum cytokine measurements

Mouse serum Il-13 and Il-6 were performed using assay kits from Meso Scale Discovery (#K152UBK and #K152QXD) according to the manufacturer instructions. Human serum samples were analyzed with the V-Plex Proinflammatory Panel 1 from Meso Scale Discovery (#K15049D) according to the manufacturer instructions.

Metabolite measurements

Serum lipids were measured using NEFA Reagent (Wako Diagnostics, #999-34691) and Infinity TG reagent (ThermoFisher, #TR22421). For measurement of muscle glycogen and triglyceride, tissues were homogenized in buffer containing 50 mM Tris, 100 mM NaCl, and 0.1% NP40. Tissue was dried using a speed-vac centrifuge and dry tissue weight was used for normalization. For glycogen content, dried tissue sample was re-suspended in KOH/Na_2SO_4 and boiled for 10 minutes. Large macromolecules were precipitated with ethanol and collected by centrifugation. Glycogen was hydrolyzed by boiling the precipitated macromolecules in H_2SO_4 for 10 minutes and neutralized with NaOH. Hydrolyzed glucose was quantified using the Glucose Oxidase Assay Kit (Sigma-Aldrich, #GAGO-20). Muscle lipids were extracted with chloroform and dried in a fume hood. Extracted lipids were analyzed using Infinity TG reagent.

Ex vivo and *in vitro* metabolic assays

Ex vivo fatty acid oxidation assays were performed using freshly isolated soleus muscle. Soleus muscle was incubated in Krebs-Ringer Hepes Buffer containing 5 mM glucose, 2% BSA and 2 μCi ^3H palmitate per muscle. Production of ^3H_2O in conditioned media

was measured to determine fatty acid oxidation and normalized to muscle weight. Fatty acid oxidation in differentiated myotubes was performed similarly. Fatty acid uptake was determined by measuring ^{3}H palmitate uptake into differentiated myotubes in 5 minutes. Fatty acid oxidation and uptake were normalized to protein content. Glucose uptake was measured by uptake of ^{3}H 2-deoxy-d-glucose in Krebs-Ringer Hepes Buffer in C2C12 myotubes.

Muscle fiber type staining

Frozen muscle sections (10 μm) were incubated in 0.2M sodium phosphate buffer, pH 7.6, containing 167 mM sodium succinate and 1.2 mM nitro blue tetrazolium for 30 minutes at 37°C. Slides were washed with diH_2O followed by 30%, 60% and 90% acetone and mounted with aqueous mounting media.

RNA-seq and analysis

RNA-seq was performed on 4 animals/genotype/group. Sequencing and raw data processing were conducted at the IMB Genomics Core and IMB Bioinformatics Service Core at the Academia Sinica (Taipei, Taiwan). Briefly, samples were quantified with Ribogreen (Life Technologies, CA) and RNA integrity was checked with a Bioanalyzer 2100 (Agilent, CA). (RIN>8; OD 260/280 and OD 260/230>1.8) RNA libraries were prepared with the TruSeq Stranded mRNA Library Preparation Kit (Illumina). Sequencing was analyzed with an Illumina NextSeq 500 instrument. Raw data was analyzed using the CLC Genomics Workbench. A significance cut-off of $p<0.05$ was used for downstream analysis. Gene Ontology was performed with DAVID

(https://david.ncifcrf.gov). *De Novo* Motif Enrichment was performed with HOMER (http://homer.ucsd.edu/homer) searching 200 bp upstream and downstream of transcription start sites with default settings.

qPCR

Relative gene expression was determined by real-time qPCR with SYBR Green. Expression was normalized to 36B4 as the internal standard. All primer sequences are listed in Table 2.4. Relative mtDNA was quantified by real time PCR using primers for mitochondrially-encoded Nd1 normalized to nuclear-encoded 36B4 DNA.

Immunoblotting

Standard Tris-Glycine SDS-PAGE was performed and transferred to PVDF membrane by wet transfer. Primary antibodies were incubated overnight in 1% BSA in TBST buffer. ECL signal was imaged using a BioRad ChemiDoc XRS+ imaging system. Antibodies for immunoblotting were anti-rat/mouse OxPhos complex kit (Invitrogen, #458099), anti-β-Tubulin (Cell Signaling, #2146), anti-Phospho-Stat3 Tyr705 (Cell Signaling, #9145), and anti-Stat3 (Cell Signaling, #12640).

Isolation of mitochondria

Mitochondria from skeletal muscle were isolated by differential centrifugation [58]. Briefly, gastrocnemius was collected, placed on ice, minced with scissors and washed three times with 1mL PBS with 10 mM EDTA. Muscle was re-suspended in isolation buffer 1 containing 70 mM sucrose, 50 mM Tris, 50 mM KCl, 10 mM EDTA, and 0.2%

fatty-acid free BSA (pH 7.4), followed by homogenization with a polytron homogenizer four times for 5 seconds each. Nuclei and large debris were removed by centrifugation at 700g for 10 minutes at 4°C. The supernatant was collected and centrifuged at 10,000g for 10 minutes at 4°C to pellet mitochondria. Mitochondria were re-suspended in buffer isolation buffer 2 containing 70 mM sucrose, 200 mM mannitol, 5 mM EGTA, and 10 mM Tris (pH 7.4) and passed through a 70μM cell strainer. Mitochondria were centrifuged again at 10,000g for 10 minutes at 4°C to remove debris and re-suspended in isolation buffer 2 or specific buffers for downstream applications.

Mitochondrial respiration and activity assays

For measuring respiration of C2C12 myotubes, myoblasts were plated (50k cells/well) and differentiated for 7 days in Seahorse XF24 microplates. An hour prior to start of the assay, myotubes were switched to DMEM (no bicarbonate) with 5 mM glucose and 1 mM pyruvate. Respiration was measured 3 times followed by injection of oligomycin (2 μM final), FCCP (1 μM), and rotenone/antimycin A (1 μM) with three measurements following each injection. Data were normalized to protein content.

Electron flow assays with isolated mitochondria were performed as described previously [59]. Isolated mitochondria (5 μg/well) were plated in XF24 microplates in buffer containing 70 mM sucrose, 220 mM mannitol, 10 mM KH_2PO_4, 5 mM $MgCl_2$, 2 mM HEPES, 1 mM EGTA and 0.2% BSA. Initial assay buffer additionally contained 10 mM pyruvate, 2 mM malate and 6 μM FCCP for complex I driven respiration. Sequential injections of 2 μM rotenone, 10 mM succinate, 4 μM antimycin a, and 100 μM TMPD/10 mM ascorbate were used to measure complex II and IV respiration.

Complex IV activity was measured using the Complex IV Rodent Enzyme Activity Microplate Assay Kit (Abcam, #AB109911) according to the manufacturer instructions using 10 µg of isolated mitochondria per well. Activity was measured by the oxidation of cytochrome c and loss of absorbance at 550 nm by reduced cytochrome c.

Luciferase reporter assays

AD293 cells were plated in 96-well plates (10k cells/well) in DMEM, 10% FBS. The next day, wells were co-transfected with 50 ng firefly luciferase reporter, 10 ng CMV-β-Galactosidase expression vector (internal control) and 10-30 ng control or Stat3 expression vector using TransIT-LT1 transfection reagent (Mirrus, #MIR2300). The media was changed 24 hours later and cells were harvested 48 hrs after transfection. Luciferase activity was measured using the Luciferase Activity Assay (Promega, #E1501) and normalized to β-Galactosidase activity.

For luciferase assays performed in C2C12 myoblasts, cells were plated in 48-well plates. Each well was transfected with 0.5 µg of firefly luciferase reporter and 30 ng Stat3 expression vector using Lipofectamine 2000 transfection reagent (Thermo Fisher, #11668019). Media was changed 24 hours later to fresh media -/+ rIL-13 for 24 hours and luciferase activity was measured using the Promega Luciferase Activity Assay.

Stat3 with an N-terminal Flag tag was cloned into the pCMX-PL1 vector containing a CMV promoter using EcoRI and XhoI restriction sites. Primer sequences can be found in Table 2.3. 1kb and 2kb promoter regions of Errα and Errγ were cloned into the pGL3-Basic vector using primer sequences provided in Table 2.3. Errα promoters were cloned starting from bases -24 to -1039 and -24 to -2027 for the 1kb and 2kb promoters

respectively, with +1 being the transcriptional start site. Errγ promoters were cloned starting from bases -108 to -1119 and -24 to -2094 for the 1kb and 2kb promoters respectively, with +1 being the transcriptional start site. For mutation of the Stat3 binding site in the Errγ 2kb promoter, site directed mutagenesis was performed using oligonucleotides provided in Table 2.3. All plasmids were sequenced to confirm sequence integrity/identity.

Statistical Analysis

All data are presented as mean ± SEM. Statistical analysis was performed using GraphPad Prism 7. For cell-based studies, comparison of two parameters was performed using two-tailed Student's t test. Multi-parameter analyses of cell-based studies were performed with Two-way ANOVA followed by Tukey post-hoc tests. Cell-based experiments were performed with 3-6 biological replicates and repeated at least 3 times. Two-parameter comparisons of samples from *in vivo* studies were performed using the Mann-Whitney test. Two-way ANOVA was used to analyze multi-parameter *in vivo* experiments. Statistical significance was defined as $p<0.05$ noted with *.

Author contributions and acknowledgments

N.H.K., K.J.S., A.L.H., M.M.C., R.K.A., Y.H.L., M.R.G., D.J., S.L. performed the experiments. C.M.P. and J.A.C. provided human serum samples. V.N. assisted in method development. N.H.K. and C.H.L. conceptualized the study, designed experiments, interpreted data and wrote the manuscript. C.H.L. supervised the study. We thank Drs. G. Hotamisligil, R. V. Farese and K. Inouye for help with

treadmill/metabolic cage studies; Drs. A. J. Wagers, J. R. Mitchell and X. Yang for critical comments; Dr. U. Unluturk for technical assistance; the IMB Genomics Core and IMB Bioinformatics Service Core at Academia Sinica (Taipei, Taiwan) for sequencing and RNA-seq data analysis.

Table 2.1. Female human subject additional data

	Obese		Normal Weight		Endurance Trained	
Parameter	Average	SEM	Average	SEM	Average	SEM
n	36	-	23	-	24	-
Age (years)	34.35	2.78	22.91	0.82	27.26	1.88
Weight (kg)	92.11	2.71	60.60	1.67	57.91	1.76
Insulin (ng/dL)	505.33	57.85	224.04	29.95	189.21	25.95
TG (mg/dL)	50.24	5.89	33.46	2.60	34.27	2.80
FFA (mM)	0.53	0.049	0.45	0.039	0.58	0.053
Cholesterol (mg/dL)	179.29	7.58	173.20	9.70	179.46	4.92

Table 2.2. Description of animal cohorts

Cohort info	No. Cohort	Age	Sex	Animal No.	Figures
WT, exercise training, 5 weeks-flow cytometry	2	16 weeks	male (1), repeated in female (1)	6/group	Fig. 2.1C-D, 2.2A-E
WT, exercise training, 5 weeks-serum, RNA	3	16 weeks	female (2), repeated in male (1)	5-7/group	Fig. 2.1B, 2.1E
WT vs. Il-13$^{-/-}$, exercise training, 5 weeks	4	20 weeks	male (2), repeated in female (2)	5-7/group	Fig. 2.1F, 2.3A, 2.5A, 2.5C-G, 2.7G, 2.4A-D, 2.6A-B
WT vs. Il-13$^{-/-}$, single bouts exercise	1	24 weeks	male	4-5/group	Fig. 2.3D-E
WT vs. Il-13$^{-/-}$, exercise respirometry	1	24 weeks	female	4/group	Fig. 2.3F-G
WT vs. skmStat3$^{-/-}$	2	24 weeks	male	12/group	Fig. 2.8F-G
WT vs. skmStat3$^{-/-}$, adGFP or adIl-13	1	24 weeks	male	6-8/group	Fig. 2.7B-F, 2.7H

All mice were in C57BL6/J background. Number of male and female mouse cohorts used in the study is indicated in parentheses.

Table 2.3. List of primer/oligonucleotide sequences for plasmid construction

Construct	Forward sequence	Reverse sequence
Flag-Stat3	GCGGAATTCAGGATGGATTACAAGGATGACGATGACAAGGCTCAGTGGAACCAGCTG	GCGCTCGAGTCACATGGGGGAGGTAGCACA
Errα 1kb promoter	GCGAGATCTGCAGCAACTTCTTCAGCC	GCGAGATCTCTGCGCATGCAAAACAGG
Errα 2kb promoter	GCGAGATCTCACTTTCAGAGGGCACAC	GCGAGATCTCTGCGCATGCAAAACAGG
Errγ 1kb promoter	GCGAGATCTGTCCTAGCCAGGTTGGACTCTTG	GCGAGATCTCTTAGCCCTTAGGGAGAC
Errγ 2kb promoter	GCGAGATCTGATAGCTCGACCGGGAGATAATCG	GCGAGATCTCTTAGCCCTTAGGGAGAC
Errγ 2kb Stat3 binding site mutant promoter	CACCCACACTCTTCTCGAGAGTCTTCCCAG	CTGGGAAGACTCTCGAGAAGAGTGTGGGTG
shStat3	GACGGATCCCGACTTTGATTTCAACTACAATTCAAGAGATTGTAGTTGAAATCAAAGTCGTTTTTTTGATATCGAATTCGCC	GGCGAATTCGATATCAAAAAAACGACTTTGATTTCAACTACAATCTCTTGAATTGTAGTTGAAATCAAAGTCGGGATCCGTC
Stat3 gRNA	CACCGGCAGCTGGACACACGCTACC	AAACGGTAGCGTGTGTCCAGCTGCC

Table 2.4. List of primer sequences used for RT-qPCR

Gene	Forward Sequence	Reverse Sequence
36b4	AGATGCAGCAGATCCGCAT	GTTCTTGCCCATCAGCACC
Acadl	ATGCAAGAGCTTCCACAGGAAA	CAGAAATCGCCAACTCAGCAAT
Acadm	ATGCCCTGGATAGGAAGACA	GAGCCTAGCGAGTTCAACCT
Acadvl	CCGGTTCTTTGAGGAAGTGAA	AGTGTCGTCCTCCACCTTCTC
Acsl1	GGCCGCGACTCCTTAAATAGC	CTCTATGCAGAATTCTCCTCCGC
Cox19	GTCGACCGCAATGAACTTCG	ACATTCACCGAAGTGGTCCAG
Cpt1b	GCAGGAGGAAGGGTAGAGTG	TCATCCAGGGTCACAAAGAA
Cyc1	TGGGGTGTCATTGCGAGAAG	GTAGCTGGGGTGCCATCATC
Errα	CTCAGCTCTCTACCCAAACGC	CCGCTTGGTGATCTCACACTC
Errγ	CTCCAGCACCATCGTAGAGGATC	GATCTCACATTCATTCGTGGCTG
Gbe1	CATCACCACGGAATGGGTCA	TCTGGGTACAACGTGTGAGC
Grpel1	CAGAACCTGGACGAGGACTT	CACGTTTGTATTTTTCCATGGTCT
Hadhb	TGGGAGCTGGCTTCTCTGAT	TGTGGTCATGGCTTGGTTTG
Hk2	ACATTGTGGCTGTGGTGAAT	CTGCCAGTACCCACAATGAG
Idh2	CACCCGCCATTACCGAGAA	CAGCGTCTGTGCAAACCTGATA
Il-13	TGGCTCTTGCTTGCCTTGGTGG	CCATACCATGCTGCCGTTGCA
Ldhb	AGAACTGGAAGGAGGTGCAT	TGGTGTAGCCTTTGAGCTTTG
Lpl	GCGTAGTTCCAGCAGCAAAG	AGAAATCTCTTCCCGCGTCTG
Lyrm7	GAGAGCATTGGAAGCAGCCAG	GAGCAATAATTCCACATCAGAACCT
Mdh1	CTGTTGGACATCACCCCCAT	GTCCGTTGCAATGACATCCTG
Nd1	AATCGCCATAGCCTTCCTAA	CACTTCGCTGATACCCCTGA
Ndufs8	CTGGGATCTAGCGCTTCGG	GCTCAGGCGATACATCACTTTC
Pdha1	GAAGATGCTTGCCGCTGTATC	CCGATGAAGGTCACATTTCTTAAT
Phkb	GGGCCAAGCGCTCAGTTTTA	GAAGGCTGCATCAGGTGAGT
Phkg1	GGAGCAAGACAGCAACTCCA	AACACCTCGTGAGGTCCTTG
Sdhb	CAGAGTCGGCCTGCAGTTTC	GGTCCCATCGGTAAATGGCA
Stat3	CATCTGTGTGACACCAACGAC	CATGTCAAACGTGAGCGACTC

Chapter 3

IL-13 signaling mediates beige fat biogenesis

Abstract

During cold exposure and exercise, β-adrenergic signaling primes the thermogenic function of brown adipose tissue, increases the abundance of multilocular beige adipocytes and stimulates fatty acid release from classical white adipocytes. Multiple studies have implicated Th2 immune signaling in thermogenesis and beige fat development, however the mechanisms driving these functions remain unclear. Unexpectedly, both Il-13$^{-/-}$ and Il-13Rα1$^{-/-}$ mice maintain their core body temperatures upon exposure to cold, suggesting that Il-13 signaling is not required for cold-induced thermogenesis. In contrast, our study demonstrates that Il-13 and its receptor Il-13Rα1 play a key role in the biogenesis of beige fat in response to β_3-adrenergic agonist treatment. Il-13Rα1$^{-/-}$ pre-adipocytes also display defects in beige adipocyte differentiation *in vitro*. The reduced beige adipogenic capacity in Il-13Rα1$^{-/-}$ mice is associated with hypertrophy of white adipose tissue and systemic insulin resistance. These results highlight the specific function of Th2 immune signaling in beige versus brown adipocytes and implicate the relevance of Il-13-mediated beige cell development in metabolic homeostasis rather than thermogenesis.

Introduction

The re-discovery of functional brown adipose tissue in humans has sparked a renewed interest in the role of adipose tissues in non-shivering thermogenesis and systemic metabolic homeostasis [60]. Adipose tissues display a wide spectrum of phenotypic characteristics influenced by genetics, anatomical location, and environmental signals [61]. Classical white fat is composed of triglyceride storing

adipocytes possessing a single large lipid droplet (unilocular). Stored triglycerides are released via lipolysis as albumin-bound free fatty acids for oxidation by peripheral tissues such as skeletal muscle. Brown fat develops from a unique lineage of myogenic factor 5 (Myf5) positive cells is enriched with mitochondria. Brown adipocytes are multilocular and express a specialized mitochondrial protein, uncoupling protein 1 (Ucp1), which generates heat for non-shivering thermogenesis. In addition to classical brown and white adipose depots, mice and humans have depots of multilocular, Ucp1 expressing beige adipocytes, which display an intermediate phenotype. Beige adipocytes reside primarily in subcutaneous adipose depots and are not derived from the same lineage as classical brown adipocytes. It is also worth noting that many of the key regulators of skeletal muscle oxidative metabolism and mitochondrial biogenesis, are shared by brown and beige adipocytes including Pgc-1α, Errα and Errγ [62-64].

Adipose tissue displays plasticity in response to environmental challenges such as cold [61]. Acutely, cold exposure triggers β-adrenergic activation of brown adipocytes leading to increases in mitochondrial activity, metabolic substrate oxidation and generation of heat by Ucp1. Chronic cold exposure triggers additional thermogenic mechanisms including an increase in the number of $Ucp1^+$ beige adipocytes in white adipose depots. Although not completely understood, it appears that both recruitment and differentiation of beige pre-adipocytes and conversion of white adipocytes contribute to the increase in beige cells during chronic cold exposure or β-adrenergic signaling activation [65]. Endurance exercise similarly activates β-adrenergic signaling and can increase beige adipose development, although the physiological function of this adaptation and the underlying mechanism are not clear [42, 66].

Several signals have been shown to drive the development of beige adipose in response to cold exposure and exercise. A myokine produced from exercising muscle, Irisin, was among the first identified signals to promote development of beige adipose tissue through directly acting on adipocytes [67]. Another factor, Meteorin-like, was identified as a muscle produced factor that increased beige adipose in mice through increasing alternative activation of adipose resident macrophages [40]. Fibroblast growth factor 21 (FGF21), a critical regulator of the fasting response, is also elevated by exercise and has potential roles in beige adipose development [68]. Treatment of cultured adipocytes with FGF21 promotes beiging, and $FGF21^{-/-}$ mice have an impaired cold-induced beiging response [69]. Atrial natriuretic peptide (ANP) and brain-type natriuretic peptide (BNP) have well characterized roles in adjusting blood volume in response to exercise training. These factors have also been shown to promote beiging of white adipose tissue and potentially support exercise-induced lipolysis [70].

In addition to canonical functions in immune responses, cytokines support a variety of adaptive metabolic responses. In lean adipose tissue, M2 macrophages polarized by Th2 cytokines promote insulin sensitivity [28, 29]. In contrast, obese adipose has an increased abundance of inflammatory cells including many M1 macrophages and other immune cell subsets [17]. Several studies have defined a role for the Th2 cytokines Il-4 and Il-13 in the thermogenic function of brown and beige adipose tissue. The early work has suggested that alternatively catecholamines derived from M2 macrophages is required for brown adipocyte activation [38]. This mechanism was recently challenged by others demonstrating that macrophages are not major producers of catecholamines [41]. Several lines of evidence support a role for Th2

signaling in development of beige adipose. Specifically, type 2 innate lymphoid cells (ILC2) were identified as key drivers of the beiging of white adipose tissue in mice and humans [36, 37, 39]. However, one report identified an Il-4R-dependent mechanism in pre-adipocytes [37], while the other found that signaling via Il-4R is not required for ILC2 induced beiging [36]. Of note, ILC2 cells are major peripheral producers of Il-13, but do not produce Il-4 [33].

We have recently identified Il-13 as an exercise-induced factor that mediates the metabolic benefits of exercise training. Il-13 regulates the adaptation of skeletal muscle to endurance training by promoting oxidative metabolism in skeletal muscle. Based on this observation, we seek to determine whether Il-13 is also critical in the metabolic adaptation of adipose tissues characterized by beiging and thermogenesis. Our results suggest that Il-13 signaling regulates beige cell activation but is dispensable for cold-induced thermogenesis.

Results

Il-13 is not required for brown adipose tissue mediated thermogenesis

To assess the role of Il-13 in the thermogenic response to environmental cold exposure, we examined the body temperature and metabolic response of wild-type (WT) and Il-13 knockout (Il-13$^{-/-}$) mice at different ambient temperatures using implanted thermometers and indirect calorimetry. Animals were housed in metabolic chambers at thermoneutrality (30°C), room temperature (22°C), and cold (4°C) for 3 days each. Oxygen consumption is used as an overall readout of total metabolic activity. As expected, oxygen consumption was greatest in the cold, and was lowest at

thermoneutrality (Fig. 3.1A). The typical day-night fluctuations in respiration corresponding with the mouse circadian fasting-feeding cycle were also evident. However, there was no difference in oxygen consumption or core body temperature between WT and Il-13$^{-/-}$ mice in each of the three temperatures (Fig. 3.1B-1C). Respiratory exchange ratio (VO_2/VCO_2) (RER) can be used to estimate metabolic substrate utilization. There was no significant change in RER between WT and Il-13$^{-/-}$ mice, although Il-13$^{-/-}$ mice displayed a trend towards having elevated RER in colder temperatures during the light cycle (Fig. 3.1D). This elevation in RER correlated with increases in food consumption (Fig. 3.1E). Brown adipose tissue is a major contributor to non-shivering thermogenesis in mice during cold exposure. We found that brown adipose of Il-13$^{-/-}$ mice expresses normal amounts of Ucp1 compared to WT brown adipose (Fig. 3.1F).

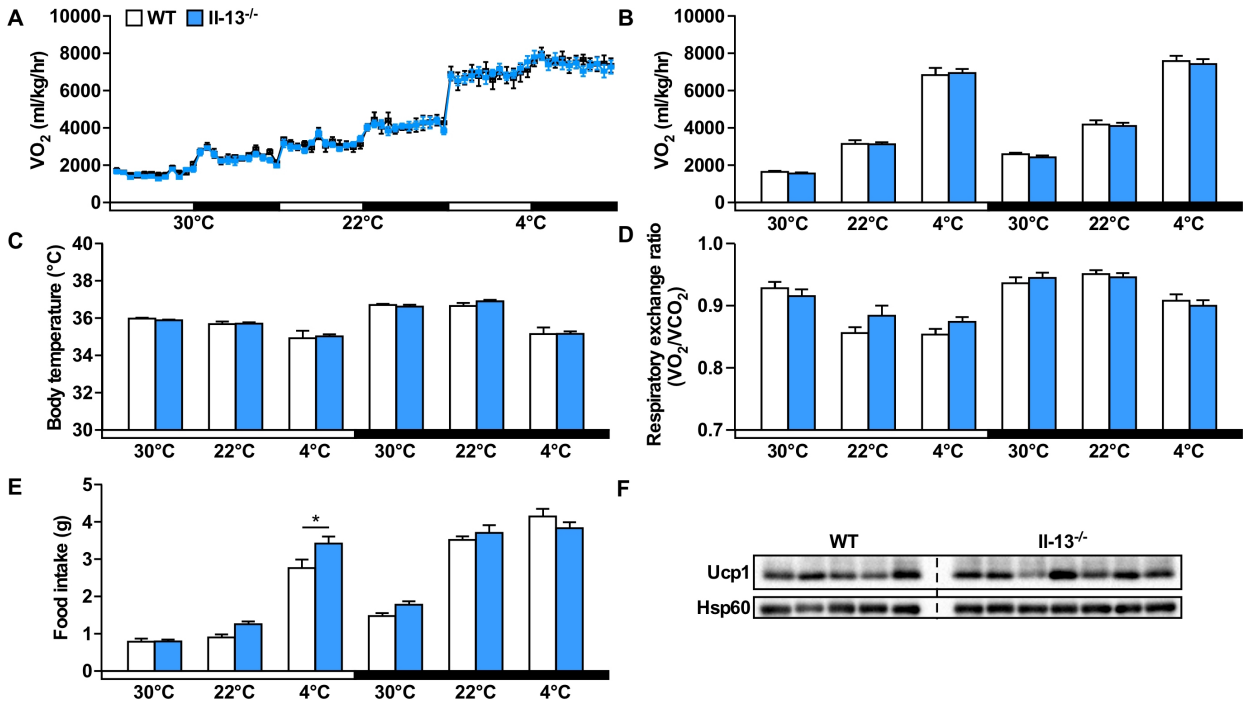

Figure 3.1. The Th2 cytokine Il-13 is not required for thermogenesis or brown fat development. (A) Respiration (VO_2) of WT and Il-13$^{-/-}$ mice housed at thermoneutrality (30°C), room temperature (22°C) and cold (4°C). White and black bars indicate light and dark cycles times, respectively. (B) Average respiration (VO_2) of WT and Il-13$^{-/-}$ mice housed at thermoneutrality (30°C), room temperature (22°C) and cold (4°C). (C) Average body temperature of WT and Il-13$^{-/-}$ mice housed at thermoneutrality (30°C), room temperature (22°C) and cold (4°C) measured by temperature probe implanted in peritoneum. (D) Average respiratory exchange ratio of WT and Il-13$^{-/-}$ mice housed at thermoneutrality (30°C), room temperature (22°C) and cold (4°C). (E) Food intake of WT and Il-13$^{-/-}$ mice housed at thermoneutrality (30°C), room temperature (22°C) and cold (4°C). (F) Protein expression of Ucp1 in brown adipose tissue of WT and Il-13$^{-/-}$ mice measured by western blot. N=5-7, 20 weeks old male mice. Data presented as mean ± SEM. *$p<0.05$

Il-13 shares a heterodimeric receptor with another cytokine, Il-4, which is composed of Il-13Rα1 and Il-4R. To further characterize the role of Th2 signaling in thermogenesis, we performed similar metabolic monitoring to the experiment described in Fig. 3.1 using WT and Il-13Rα1$^{-/-}$ mice. Like Il-13$^{-/-}$ mice, Il-13Rα1$^{-/-}$ mice had similar rates of oxygen consumption at each of the three examined environmental temperatures (Fig. 3.2A-B) and did not show any defect in maintaining body temperature compared to WT control mice (Fig. 3.2C). RER was not different between genotypes (Fig. 3.2D), however, Il-13Rα1$^{-/-}$ mice ate more food during the light cycle when exposed to cold (Fig. 3.2E). The brown adipose tissue of Il-13Rα1$^{-/-}$ mice expressed normal levels of Ucp1 protein. Collectively, these data demonstrate that Il-13/Il-13Rα1 signaling is not required for normal development of brown adipose tissue and thermogenic response to cold.

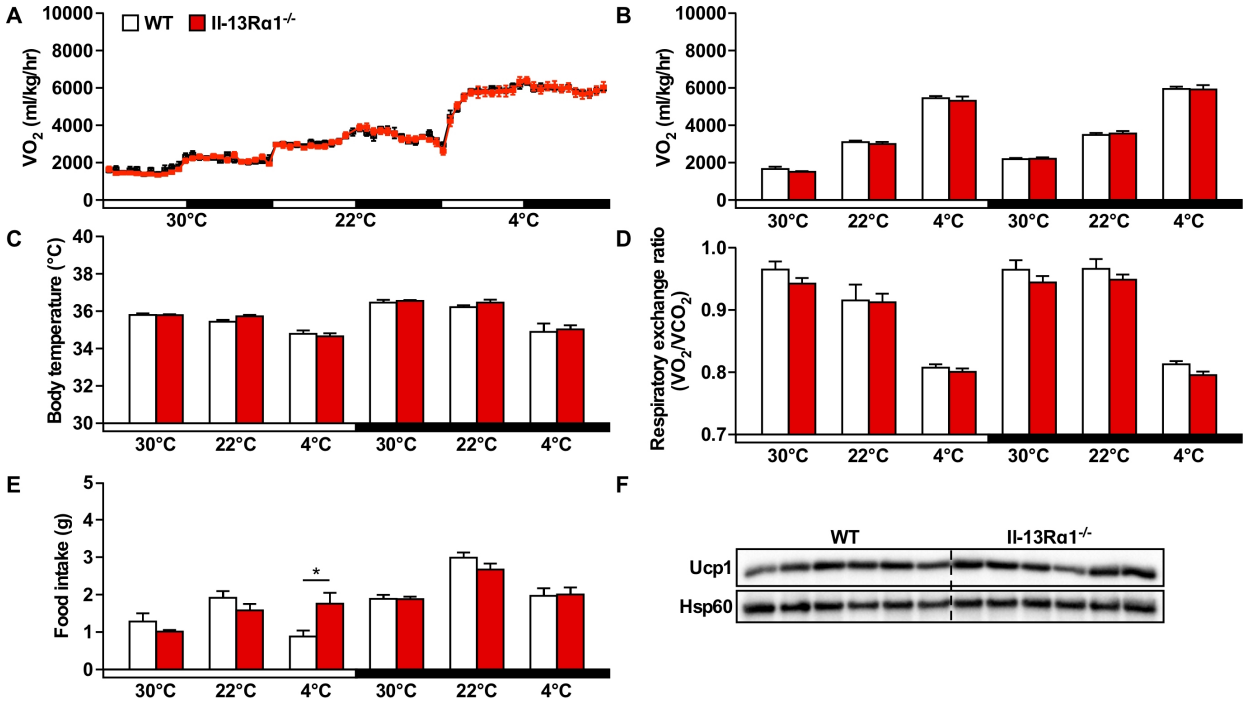

Figure 3.2. Signaling via Il-13Rα1 is not required for thermogenesis or brown fat development. (A) Respiration (VO_2) of WT and Il-13Rα1$^{-/-}$ mice housed at thermoneutrality (30°C), room temperature (22°C) and cold (4°C). White and black bars indicate light and dark cycles times, respectively. (B) Average respiration (VO_2) of WT and Il-13Rα1$^{-/-}$ mice housed at thermoneutrality (30°C), room temperature (22°C) and cold (4°C). (C) Average body temperature of WT and Il-13Rα1$^{-/-}$ mice housed at thermoneutrality (30°C), room temperature (22°C) and cold (4°C) measured by temperature probe implanted in peritoneum. (D) Average respiratory exchange ratio of WT and Il-13Rα1$^{-/-}$ mice housed at thermoneutrality (30°C), room temperature (22°C) and cold (4°C). (E) Food intake of WT and Il-13Rα1$^{-/-}$ mice housed at thermoneutrality (30°C), room temperature (22°C) and cold (4°C). (F) Protein expression of Ucp1 in brown adipose tissue of WT and Il-13Rα1$^{-/-}$ mice measured by western blot. N=5-7, 24 weeks old male mice. Data presented as mean ± SEM. *$p<0.05$

Il-13 regulates beige adipose development and metabolic homeostasis

Although brown adipose tissue functioned normally in both Il-13$^{-/-}$ and Il-13Rα1$^{-/-}$ mice, the consistent increase in food consumption during the light cycle suggests that Il-13 signaling deficient mice may compensate for minor thermogenic defects by increasing food consumption. We examined the weight of different adipose depots in both Il-13$^{-/-}$ and Il-13Rα1$^{-/-}$ mice. There was an increase in white adipose depots (epididymal and inguinal) of Il-13$^{-/-}$ and Il-13Rα1$^{-/-}$ mice, while the brown adipose tissue weight was not different (Fig. 3.3A). Similar to Il-13$^{-/-}$ mice [31], Il-13Rα1$^{-/-}$ mice had reduced glucose tolerance as demonstrated by glucose tolerance test (GTT) (Fig. 3.3B). Insulin tolerance test (ITT) further revealed that Il-13Rα1$^{-/-}$ mice had reduced insulin sensitivity (Fig. 3.3C), suggesting that dysregulated white adipose tissue homeostasis is associated with a systemic metabolic phenotype.

Studies by others suggest a potential role of Th2 signaling in beige cell development at the pre-adipocyte stage [37], however the specific role of Il-13 and its receptor Il-13Rα1 in mature adipocytes has not been investigated. The recruitment of beige adipocytes in mature mice can be induced by injecting mice with the β_3-adrenergic receptor agonist CL316,243. After 10 days of CL316,243 treatment, adipose tissue were collected and the development of beige fat examined by histology and protein expression of Ucp1. CL316,243 treatment reduced the overall adipocyte cell size and greatly increased the appearance of multilocular beige cells in inguinal adipose tissue (Fig. 3.3D). Il-13$^{-/-}$ mice exhibited larger adipocytes in inguinal adipose tissue that were resistant to CL316,243 induced beiging. Expression of Ucp1 in inguinal adipose tissue was greatly up-regulated in WT mice by CL316,243, while this response was

blunted in Il-13$^{-/-}$ mice (Fig. 3.3E). A similar defect was observed in CL316,243 treated Il-13Rα1$^{-/-}$ mice as seen by H&E staining compared to WT mice (Fig. 3.3F). Il-13Rα1$^{-/-}$ was also required for increased Ucp1 protein expression in inguinal adipose tissue in response to CL316,243 (Fig 3.3G). These data indicate that Il-13 signaling mediates the recruitment and development of beige adipocytes. These cells appear to play a predominant role in metabolic homeostasis than in thermogenic potential.

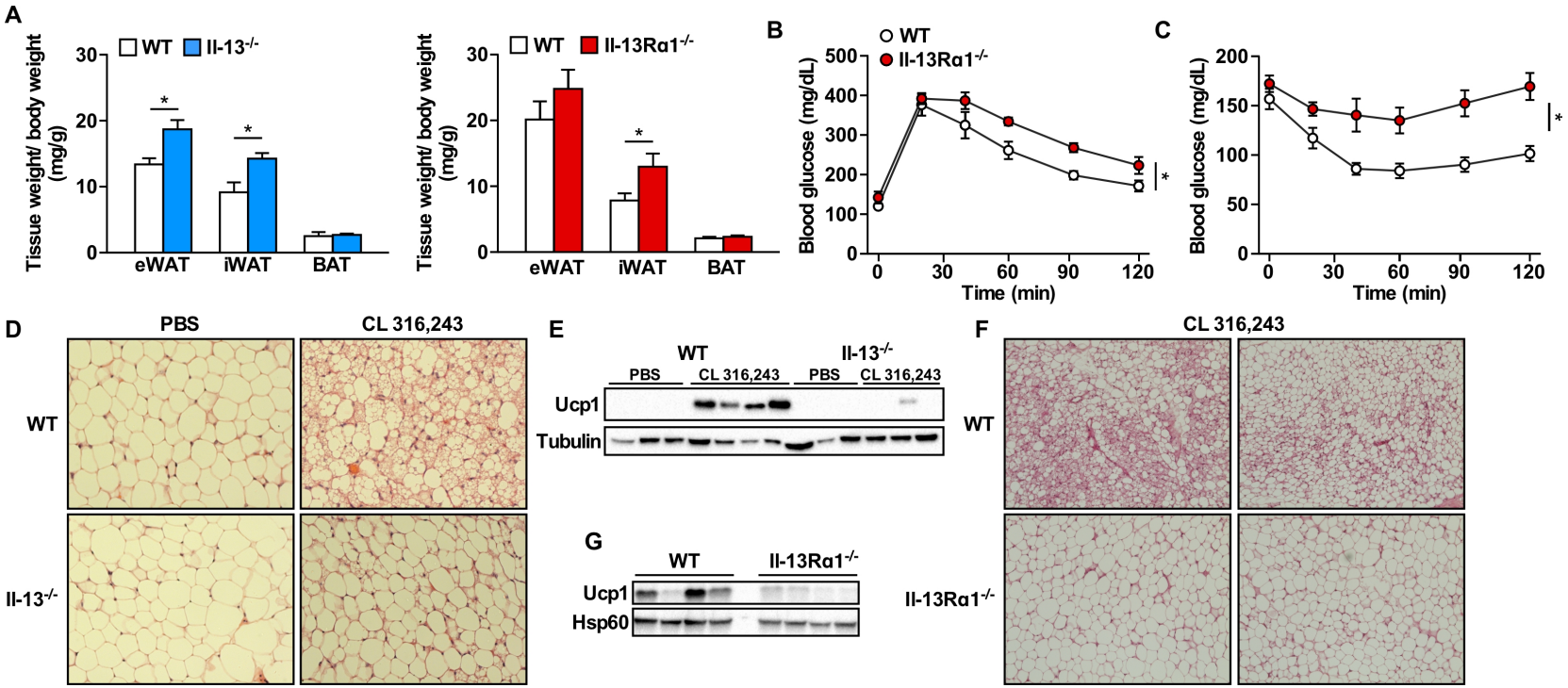
A
WT
Il-13-/-
Tissue weight/ body weight (mg/g)
eWAT
iWAT
BAT
WT
Il-13Rα1-/-
B
WT
Il-13Rα1-/-
Blood glucose (mg/dL)
Time (min)
C
Blood glucose (mg/dL)
Time (min)
D
PBS
CL 316,243
WT
Il-13-/-
E
WT
Il-13-/-
PBS
CL 316,243
PBS
CL 316,243
Ucp1
Tubulin
F
CL 316,243
WT
Il-13Rα1-/-
G
WT
Il-13Rα1-/-
Ucp1
Hsp60

Figure 3.3. Il-13/Il-13Rα1 signaling supports the development of beige adipocytes in inguinal adipose tissue. (A) Masses of epididymal (eWAT), inguinal (iWAT) and brown (BAT) adipose tissues from WT, Il-13Rα1$^{-/-}$ and Il-13$^{-/-}$ mice. N=5-7, 20-24 weeks old male mice. (B) Glucose tolerance test of WT and Il-13Rα1$^{-/-}$ mice. N=5-6, 20 weeks old male mice. (C) Insulin tolerance test of WT and Il-13Rα1$^{-/-}$ mice. N=5-6, 20 weeks old male mice. (D) H&E staining of inguinal adipose from WT and Il-13$^{-/-}$ mice injected with PBS or CL316,243 for 10 days. (E) Protein expression of Ucp1 in inguinal adipose from WT and Il-13$^{-/-}$ mice injected with PBS or CL316,243 for 10 days. (F) H&E staining of inguinal adipose from WT and Il-13Rα1$^{-/-}$ mice injected with CL316,243 for 10 days. (G) Protein expression of Ucp1 in inguinal adipose from WT and Il-13Rα1$^{-/-}$ mice injected with CL316,243 for 10 days. Data presented as mean ± SEM. *$p<0.05$

Th2 cytokine signaling promotes beige adipocyte development and pre-adipocyte maintenance

To dissect mechanisms of Il-13-Il-13Rα1 signaling in beige cell biology, we established *in vitro* models of pre-adipocytes from inguinal, epididymal and brown adipose tissues of WT and Il-13Rα1$^{-/-}$ mice. Pre-adipocytes from different adipose depots exhibited distinct characteristics such as cell size, lipid droplet number and lipid droplet size (Fig. 3.4A and data not shown). Adipocytes differentiated from epididymal pre-adipocytes were large and had few large lipid droplets. In contrast, those differentiated from brown adipose pre-adipocytes were much smaller in size and had many small lipid droplets. Differentiated adipocytes derived from the inguinal adipose tissue had an intermediate phenotype between those of epididymal and brown adipose derived cells. Since inguinal adipose tissue (iWAT) displays the most capacity for beiging, we focused our analysis on this fat depot. iWAT pre-adipocytes were immortalized using retrovirus containing the SV40 large T antigen. We isolated single clones that exhibited 100% differentiation capacity for downstream analysis. Il-13Rα1$^{-/-}$ iWAT adipocytes accumulated more triglyceride compared to WT iWAT cells (Fig 3.4B-C). Furthermore, Il-13Rα1$^{-/-}$ iWAT adipocytes had reduced Ucp1 protein expression and uncoupled respiration (Fig 3.4D-E). These observations were consistent with defects seen in beige adipogenesis *in vivo* and indicate that iWAT pre-adipocytes from Il-13Rα1$^{-/-}$ mice have reduced capacity to become beige adipocytes. We also measured CL316,243-induced lipolysis by measuring glycerol release and found that Il-13Rα1$^{-/-}$ iWAT adipocytes were less responsive to the β_3-adrenergic agonist (Fig. 3.4F). Next, we tested whether there were differences in β-adrenergic signaling in Il-13Rα1$^{-/-}$ iWAT

adipocytes. Interestingly, Il-13Rα1$^{-/-}$ iWAT adipocytes showed normal signaling responses to CL316,243, as measured by phosphorylation of hormone sensitive lipase (HSL) and protein kinase A (PKA) substrates (Fig 3.4G), suggesting that the defect is not at the β_3-adrenergic signaling level.

One mechanism of beige fat biogenesis is development of beige adipocytes from adipocyte precursor cells in response to β-adrenergic activation. Multiple studies have demonstrated that the number of pre-adipocytes greatly decreases as mice reach maturity. This is suggested as the reason why younger mice more readily develop beige adipose tissue in response to β-adrenergic stimulation by cold exposure or exercise training. Since β-adrenergic signaling was similar in WT and Il-13Rα1$^{-/-}$ adipocytes, we asked whether differences in beige adipogenesis were due to changes in the beige adipocyte precursor population. To investigate this possibility, we isolated pre-adipocytes from the inguinal adipose tissue of WT and Il-13$^{-/-}$ mice at different ages. As expected, WT mice displayed a gradual reduction in pre-adipocyte cell number per gram adipose as mice aged from 8 to 16 weeks of age (Fig. 3.4H). In contrast, Il-13$^{-/-}$ mice had far fewer pre-adipocytes at 8 weeks of age, which remained relatively unchanged, indicating that Il-13 may support maintenance of the adipocyte precursor pool as previously suggested [37].

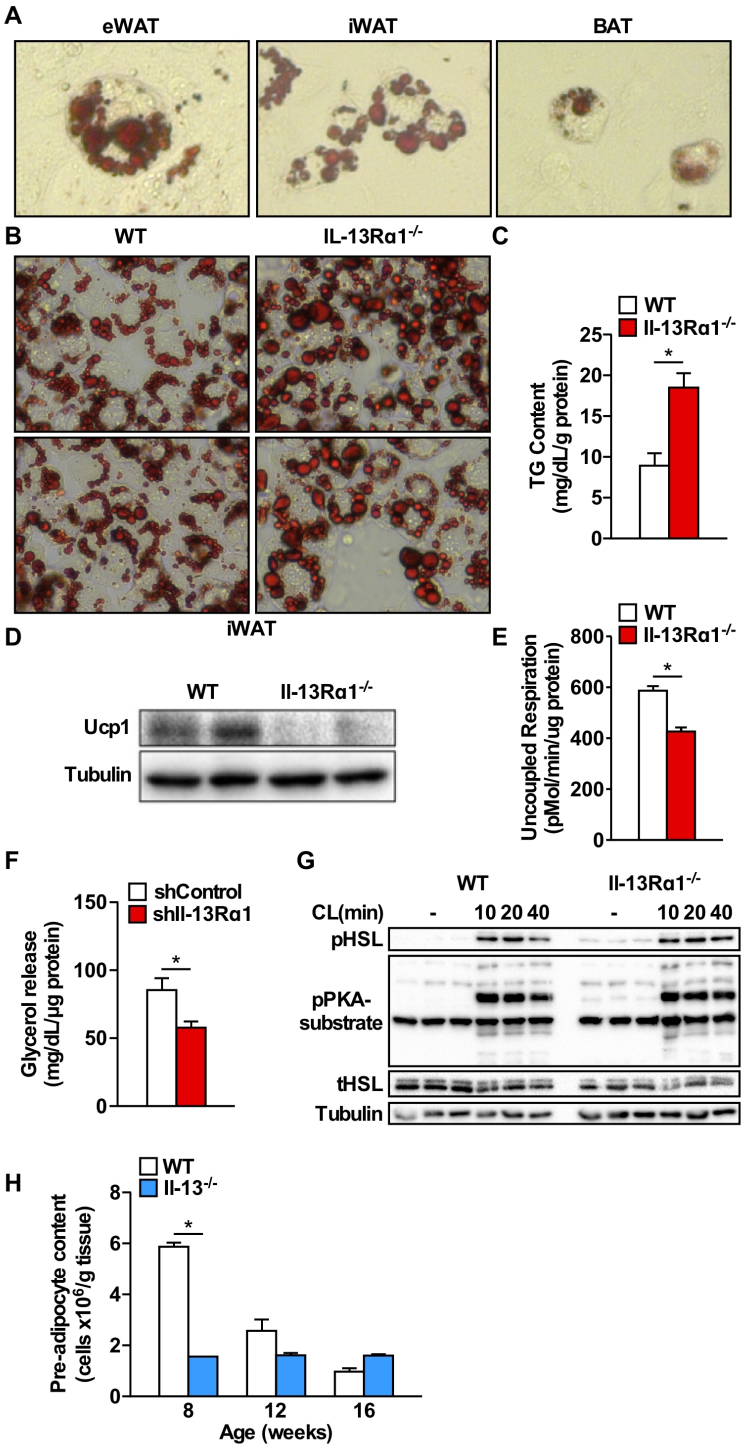

Figure 3.4. Il-13/Il-13Rα1 signaling promotes differentiation of beige adipocytes without compromising β-adrenergic signaling. (A) Representative images of

(Figure 3.4 Continued) differentiated primary adipocytes from epididymal (eWAT), inguinal (iWAT) and brown (BAT) adipose tissues stained with Oil Red O. (B) Oil Red O staining of iWAT adipocytes differentiated from immortalized pre-adipocytes of WT and Il-13Rα1$^{-/-}$ mice. (C) Triglyceride (TG) content of iWAT adipocytes differentiated from immortalized pre-adipocytes of WT and Il-13Rα1$^{-/-}$ mice. (D) Protein expression of Ucp1 in iWAT adipocytes differentiated from immortalized pre-adipocytes of WT and Il-13Rα1$^{-/-}$ mice measured by western blot. (E) Uncoupled respiration measured by seahorse bioanalyzer in iWAT adipocytes differentiated from immortalized pre-adipocytes of WT and Il-13Rα1$^{-/-}$ mice. (F) Lipolysis assay of glycerol release from shControl and shIl-13Rα1 iWAT adipocytes differentiated from immortalized pre-adipocytes of WT mice. Lipolysis was stimulated with 1μM CL316,243 for 3 hours and glycerol content was measured in the spent media. (G) Acute β_3-adrenergic stimulation of iWAT adipocytes differentiated from immortalized pre-adipocytes of WT and Il-13Rα1$^{-/-}$ mice with CL316,243 (1μM) for indicated times. Phosphorylation of hormone sensitive lipase (pHSL) and phosphorylation of PKA substrates (pPKA-substrate) were measured by western blot. (H) Pre-adipocyte number in inguinal adipose tissue of WT and Il-13$^{-/-}$ mice of various ages normalized to tissue weight. Data presented as mean ± SEM. *$p<0.05$

Discussion

Our study supports the notion that Th2 cytokines, especially Il-13, act on pre-adipocytes and adipocytes to directly enhance beiging rather than through alternatively activated macrophages. Specifically, we have shown that Il-13/Il-13Rα1 signaling is required for the development of beige adipose tissue in response to β_3-adrenergic agonist (Fig 3.5). This regulation occurs in part through promoting beige identity in differentiating adipocytes and maintaining the pool of undifferentiated pre-adipocytes. Although, Il-13 is a critical regulator of beige adipose, it is not required for mice to survive in the cold. The brown adipose tissue of mice lacking either Il-13 or Il-13Rα1 function normally and express normal levels of Ucp1 protein. This uncoupling of thermogenesis and beige adipose development indicates that beige adipose possesses functions independent of heat production.

Endurance exercise training promotes beiging of white adipose tissues through adrenergic signaling [42]. A key feature of endurance trained muscle is the increased capacity to utilize fatty acids as a fuel source. During exercise, fatty acids are released from white adipose tissue through adrenergic signaling. Our recent work highlights the role of Il-13 signaling in the metabolic adaptation of muscle to endurance training. Increased Il-13 production during endurance training may promote beiging of white adipose tissue as a mechanism to increase metabolic efficiency by enhancing fatty acid release through lipolysis for oxidation in muscle. Endurance training enhanced Il-13 production by muscle resident type 2 innate lymphoid cells (ILC2), a major source of Il-13. ILC2 cells regulate beige adipogenesis in mice and humans in part through their activation by Il-33 [36, 37]. The upstream signal activating ILC2 during exercise training

is unknown, however recent studies highlighting the activation of ILC2 by neuronal signals suggest that adrenergic signaling could directly activate Il-13 production by ILC2 cells [71-73]. Il-33 represents another candidate ILC2 activator that may act as an exercise-induced circulating regulator of beige adipogenesis. It is unknown whether Il-33 production is altered by exercise. Nevertheless, cross-talk between β-adrenergic signaling and local Th2 signaling provides a mechanism for fine-tuning the number of activated beige adipocytes in response to different stimuli. Future studies will be needed to examine whether Il-13 signaling is required for the exercise-induced beiging of white adipose tissue.

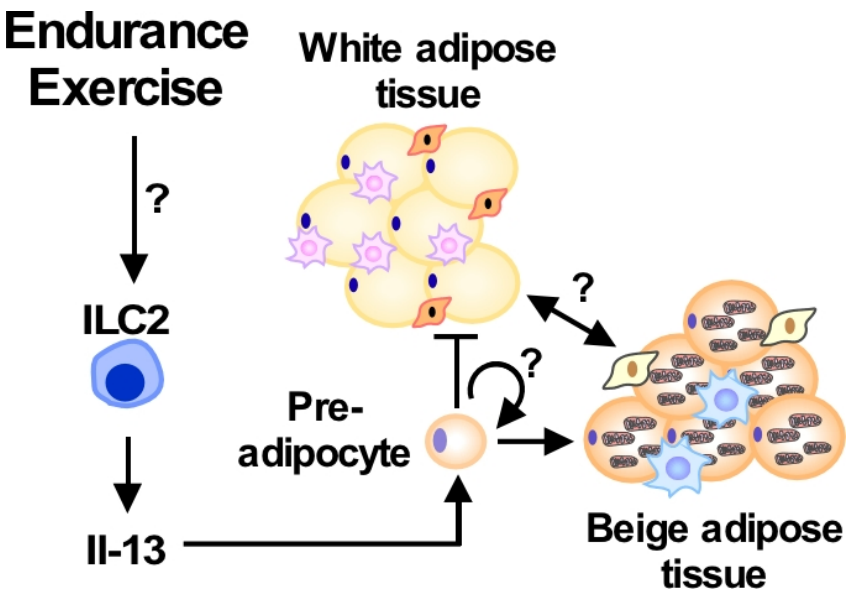

Figure 3.5. Il-13 signaling through Il-13Rα1 promotes beiging of inguinal adipose tissue. Endurance exercise promotes Il-13 production by ILC2 cells. Signaling via Il-13Rα1 shifts the differentiation program of pre-adipocytes towards that of beige rather than white adipocytes. Il-13 may also modulate differentiation of pre-adipocytes to maintain the pool of undifferentiated precursor cells *in vivo*.

Materials and Methods

Animal studies

All animal studies were approved by the Harvard Medical Area Standing Committee on Animal Research. Mouse strains used in all experiments were in the C57Bl/6J background. Mouse genetic models were validated by both DNA genotyping and mRNA expression. Littermate controls were randomized to treatment groups based on body weight and genotype.

Il-13$^{-/-}$ mice in the Balb/c background were obtained from Dr. A. McKenzie. Generation of Il-13$^{-/-}$ animals in the C57Bl/6J background was described previously [31]. These animals have been backcrossed >9 generations to C57Bl/6J mice from The Jackson Laboratory.

Il-13Rα1$^{-/-}$ animals were generated from targeted Il13ra1$^{tm1a(EUCOMM)Hmgu}$ ES cells (KO first allele) derived from the European Conditional Mouse Mutagenesis Program (EUCOMM). These ES cells were of C57Bl/6N background. ES cells were injected at the Boston Nutrition and Obesity Research Center Transgenic Core at the Beth Israel Transgenic Mouse Facility. Chimeras were bred to C57Bl/6J mice from The Jackson Laboratory. Il-13Rα1$^{-/-}$ mice were further back-crossed to C57Bl/6J animals for >8 generations and SNP genotyping was used to selectively breed animals displaying the highest inheritance of C57Bl/6J alleles [74].

Metabolic monitoring and cold challenge

All experiments were performed at the Brigham and Women's Hospital Metabolic Core. Mice were implanted with temperature probes in the peritoneum and allowed to recover

for one week before the experiment began. Mice were housed in a Comprehensive Laboratory Animal Monitoring System (CLAMS) from Columbus Instruments. Environmental temperature was placed at 30°C (thermoneutrality), followed by 22°C (room temperature), and 4°C (cold) for 3 days each. Body temperature, VO_2, VCO_2, food consumption, and activity were measured throughout the experiment.

Glucose and insulin tolerance

Mice were fasted overnight prior to glucose or insulin tolerance tests. Fasting blood glucose was measured and animals were injected with glucose (1.5 g/kg body weight) or insulin (1 U/kg body weight) into the peritoneum. Blood glucose was measured at 20, 40, 60, 90 and 120 minutes post injection.

Induction of beige adipogenesis by CL 316,243 treatment

Mice were injected in the peritoneum daily with 1mg/kg body weight CL 316,243 or equal volume PBS for 10 days.

Histology

Adipose tissues were collected, fixed in Bouin's Solution, embedded in paraffin, sectioned and processed for hematoxylin and eosin staining.

Immunoblotting

Standard Tris-Glycine SDS-PAGE was performed and transferred to PVDF membrane by wet transfer. Primary antibodies were incubated overnight in 1% BSA in TBST buffer.

ECL signal was imaged using a BioRad ChemiDoc XRS+ imaging system. Antibodies for immunoblotting were anti-Ucp1 (Abcam, #23841), anti-β-Tubulin (Cell Signaling, #2146), anti-phospho-HSL (Cell Signaling, #4126), anti-HSL (Cell Signaling, #4107), anti-phospho-PKA substrate (Cell Signaling, #9624), and anti-Hsp60 (Abcam, #45134).

Generation of adipocyte cell lines and culture conditions

Pre-adipocytes were isolated from epididymal, inguinal and brown adipose tissue stromal vascular fractions by digesting minced tissues with low glucose DMEM containing 2 mg/mL collagenase type II and 2% bovine serum albumin (BSA) for 30-60 minutes. Cells were passed through a 70μM cell strainer and washed twice with DMEM with 2% BSA and plated in DMEM with 10% fetal bovine serum (FBS). Cells were maintained in DMEM with 10% fetal bovine serum (FBS).

Pre-adipocytes from each depot were immortalized by infecting cells with retrovirus containing the SV40 Large T antigen twice. Individual clones were selected for differentiation capacity by plating at limiting dilution followed by a second round of selection by colony formation and isolation using cloning rings. Cell lines that displayed ~100% differentiation capacity by oil red O staining were selected from each depot for downstream analysis. shControl and shIl-13Rα1 iWAT cell lines were generated in iWAT pre-adipocyte cells using pSiren-RetroQ vector and retrovirus packaging system as described in Chapter 2.

Triglyceride measurement

Triglyceride content was measured by lysing cells in buffer containing 50 mM Tris pH 7.4, 100 mM NaCl, and 0.1% NP40 and measuring triglyceride with the Trinity TG reagent (Thermo Fisher). Triglyceride content was normalized to protein content.

Glycerol release assay

Differentiated adipocytes were switched to DMEM containing only 1mM glucose and sodium bicarbonate and stimulated with 1 μM CL 316,243. Media was collected at baseline and after each hour for measurement of glycerol content with the Trinity TG reagent (Thermo Fisher), which reacts with freed glycerol.

Assessment of uncoupled respiration

Uncoupled respiration was measured using the Seahorse Analyzer. Briefly, adipocytes were differentiated in a Seahorse XF24 microplate for 6 days. Adipocyte media was switched to DMEM without sodium bicarbonate or glucose/pyruvate. Uncoupled respiration was quantified by subtracting oligomycin sensitive (ATP-coupled) respiration and antimycin A insensitive (non-mitochondrial) respiration from basal respiration. Respiration was normalized to protein content.

Flow cytometry of pre-adipocytes

Adipose tissues were harvested and weighed followed by isolation of stromal vascular fractions for counting and staining with antibodies for flow cytometry. For each sample, $1x10^6$ cells were blocked and stained with viability dye followed by Cd45-APC-Cy7,

F4/80-PerCP/Cy5.5, Pdgfrα-FITC, Sca1-PE-Cy7, and Cd31-e450. Pre-adipocytes were defined as $CD45^-$, $CD31^-$, $Sca1^+$, $Pdgfr\alpha^+$ cells. Total cell number was calculated based on total cell count and tissue mass.

Statistical Analysis

All data are presented as mean ± SEM. Statistical analysis was performed using GraphPad Prism 7. For cell-based studies, comparison of two parameters was performed using two-tailed Student's t test. Multi-parameter analyses of cell-based studies were performed with Two-way ANOVA followed by Tukey post-hoc tests. Cell-based experiments were performed with 3-6 biological replicates and repeated at least 3 times. Two-parameter comparisons of samples from *in vivo* studies were performed using the Mann-Whitney test. Two-way ANOVA was used to analyze multi-parameter *in vivo* experiments. Statistical significance was defined as $p<0.05$ noted with *.

Author contributions and acknowledgments

Nelson H. Knudsen, Hyunji J. Cho, Alexander L Hyde, and Alexandra Yesian performed *in vivo* experiments with Il-$13^{-/-}$ and Il-13Rα$1^{-/-}$ mice. Nelson Knudsen generated Il-13Rα$1^{-/-}$ mice. Nelson H. Knudsen, Mayer M. Chalom, Alexander L Hyde, and Alexandra Yesian generated pre-adipocyte cell lines and performed *in vitro* experiments. Nelson H. Knudsen, Hyunji J. Cho, Alexandra Yesian and Chih-Hao Lee conceptualized the study, designed experiments, and interpreted data. Chih-Hao Lee supervised the study. Metabolic cage experiments were performed at the Brigham and Women's Hospital Metabolic Core supervised by Alex S. Banks with assistance from

Katherine Leclair, Amir Mina and Dimitrije Cabarkapa. ES cells with Il-13Rα1 targeting allele were obtained from European Mouse Mutant Cell Repository (EuMMCR) and knockout mice were generated with the help of the transgenic core of Boston Nutrition Obesity Research Center.

Chapter 4

Discussion and Conclusion

Summary of findings

In the preceding chapters I outlined immune signaling mechanisms that drive the adaptation of skeletal muscle to exercise training and development of beige fat. These mechanisms converge on local Il-13 production by ILC2 cells in skeletal muscle and adipose tissue to increase mitochondrial respiration in each tissue. Studies in macrophages identified mitochondrial oxidative metabolism as a characteristic of M2 macrophages polarized by Il-4/Il-13[75]. Our studies expand the regulation of mitochondrial biogenesis by Il-13 in immune cells to key metabolically active tissues. Il-13 signaling promotes efficient metabolic substrate utilization in muscle by enhancing fatty acid uptake and oxidation, promoting glycogen storage and increasing mitochondrial respiratory capacity. In white adipose tissue, Il-13 supports development of mitochondria-rich beige adipocytes. Therefore, Il-13 is a major mediator of tissue metabolic adaptation through communication between local immune cells, skeletal muscle and beige adipose tissue.

In the final sections, I will outline several preliminary hypotheses and future directions. Exercise training is known to increase protein translation [76] and mitochondrial respiratory complex and supercomplex activity in skeletal muscle [77]. These metabolic adaptations occur in addition to the transcriptional response. Preliminary studies indicate that Stat3 localizes to mitochondria to interact with respiratory complexes and increase their activity in response to Il-13 signaling during exercise. Il-13 also appears to enhance mitochondrial protein translation in myotubes.

Non-genomic functions of Stat3 in Il-13 mediated exercise physiology

In addition to its canonical role as a transcription factor, Stat3 localizes to mitochondria and supports respiration [78]. Overexpression of a mitochondria-targeted Stat3 protects cardiac muscle from ischemic damage through enhancing mitochondrial complex I activity [79]. Isolated mitochondria from Stat3$^{-/-}$ liver and heart display defects in electron transport chain complexes I-IV [78]. Furthermore, targeting of Stat3 to mitochondria has been proposed to occur through phosphorylation of serine 727 of Stat3 through overexpression studies [78, 80]. Although Stat3 localization has been described in several cell types, the mechanism driving its import to mitochondria remains unclear.

To determine whether Il-13 or Il-6, another Stat3-activating cytokine implicated in exercise physiology, regulates mitochondrial Stat3 function, subcellular fractionation of C2C12 myotubes was used to compare the localization of the transcriptionally active, tyrosine 705 phosphorylated Stat3 and total Stat3 protein after rIl-13 and rIl-6 treatment. As expected, rIl-6 treatment increased nuclear phospho-Stat3, which returned to baseline levels after one hour (Fig 4.2A). rIl-13 treatment increased nuclear phospho-STAT3 at 2 hrs, and also increased total Stat3 abundance in mitochondria (Fig 4.2A). In contrast, IL-6 treatment did not alter mitochondrial Stat3 abundance.

We next isolated mitochondria from skeletal muscle of mice injected with adenovirus containing either GFP or Il-13. Blue Native PAGE (BN-PAGE) was used to separate the mitochondrial respiratory complexes and supercomplexes to examine the localization of mitochondrial Stat3 (Fig 4.2B). adIl-13 increased the abundance of STAT3 in several respiratory complexes corresponding to monomeric complex IV and

supercomplexes I + III^2 and I + III^2 + IV(Fig 4.2B). The specificity of Stat3 antibody in BN-PAGE western blot was confirmed using isolated mitochondria from WT and $Stat3^{-/-}$ C2C12 myotubes (Fig 4.2C).

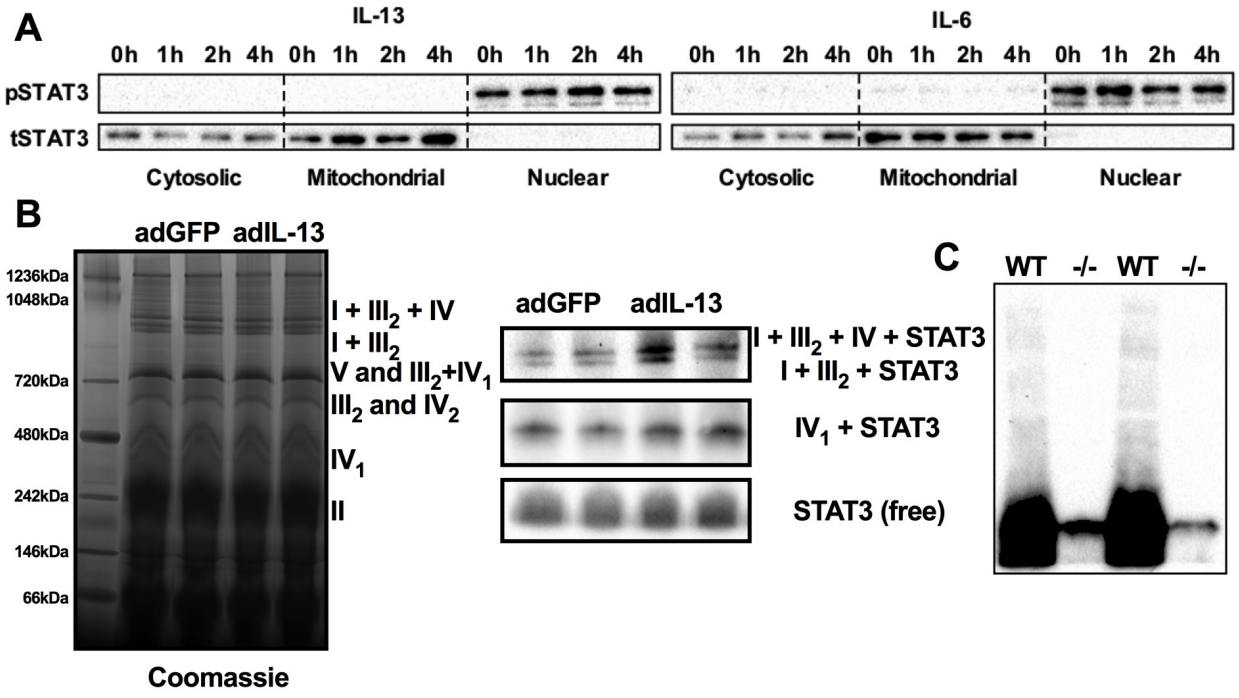

Figure 4.2. Il-13 increases mitochondrial Stat3 abundance. (A) Subcellular fractionation of C2C12 myotubes treated with rIl-13 or rIl-13 for 0-4 hours (h). Fractions were analyzed for protein abundance of tyrosine 705 phosphorylated Stat3 (pSTAT3) and total Stat3 (tSTAT3). (B) Blue Native PAGE of isolated mitochondria from gastrocnemius muscle of mice injected with adGFP or adIl-13 for 7 days. Coomassie stained gel is shown on left with various respiratory complexes labeled. Right panel shows immunoblots of BN-PAGE for Stat3 at various complex sizes. (C) BN-PAGE immunoblot for Stat3 in isolated mitochondria from WT and Stat3$^{-/-}$ C2C12 myotubes.

Mitochondria from skeletal muscle and liver of untrained and 5-week exercise trained mice were isolated for BN-PAGE analysis to examine whether exercise alters respiratory complex assembly or mitochondrial Stat3 protein levels (Fig 4.3A). Overall complex and supercomplex assembly was not altered by exercise as seen by coomassie staining; however it was clear that muscle mitochondria contain more supercomplexes than mitochondria from liver. Exercise increased the activity of complex IV (cytochrome c oxidase) containing complexes and supercomplexes in muscle but not liver (Fig 4.3B). Increased complex IV activity correlated with higher levels of complex IV-associating Stat3 (Fig 4.3C). Skeletal muscle mitochondria contained more Stat3 than liver mitochondria, including unbound (free) Stat3. These data indicate that exercise promotes Stat3 mitochondrial import and increases complex IV activity in skeletal muscle. We also show that mitochondrial Stat3 content correlates with increased mitochondrial supercomplex abundance.

Import of proteins into mitochondria requires membrane potential and thus many proteins display membrane potential dependent import kinetics. We performed subcellular fractionation after treatment with oligomycin (ATP-synthase inhibitor) and antimycin A (complex III inhibitor) to increase and reduce membrane potential, respectively. As expected, oligomycin and antimycin A treatment increased and decreased TMRE fluorescence (measurement of mitochondrial membrane potential) in C2C12 myoblasts that is associated with higer and lower mitochondrial Stat3 protein levels, respectively (Fig 4.4A-4.4B). rIl-13 treatment for one hour also increased TMRE staining, while rIl-6 treatment had no effect. Future studies will be needed to examine

how Il-13 increases mitochondrial membrane potential and whether this is required for increasing mitochondrial Stat3 abundance during exercise.

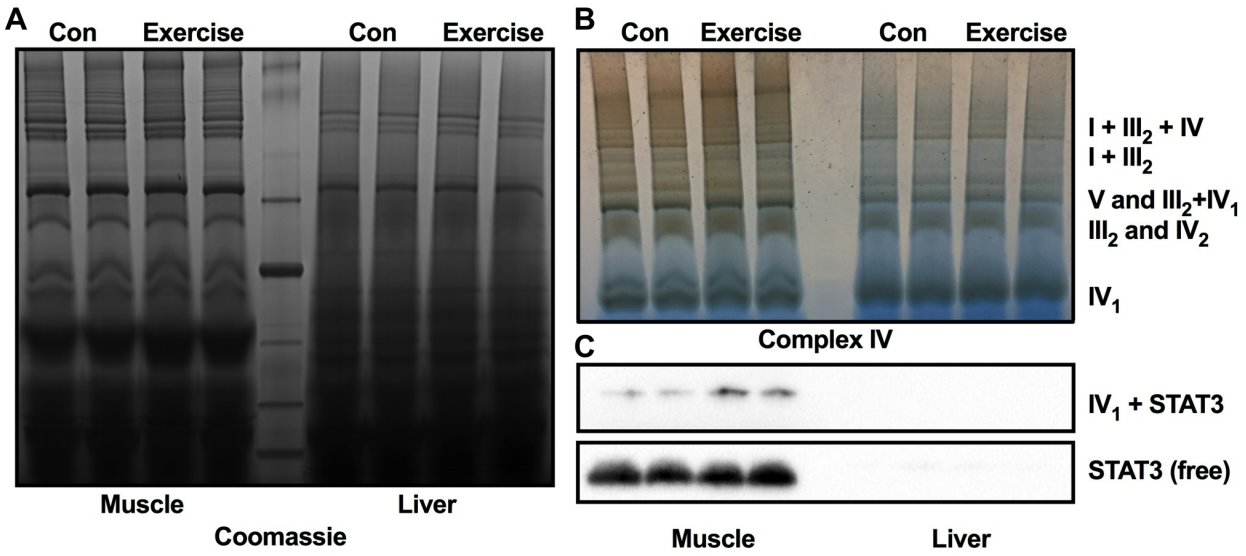

Figure 4.3. Exercise increases mitochondrial Stat3 abundance and complex IV activity. (A) BN-PAGE of isolated mitochondria from gastrocnemius muscle and liver of un-exercised and acutely exercised mice (1 hr treadmill running). BN-PAGE was stained with Coomassie stain. (B) Complex IV activity staining was performed with BN-PAGE prepared in 4.3A. (C) Immunoblots of Stat3 from BN-PAGE performed in 4.3A.

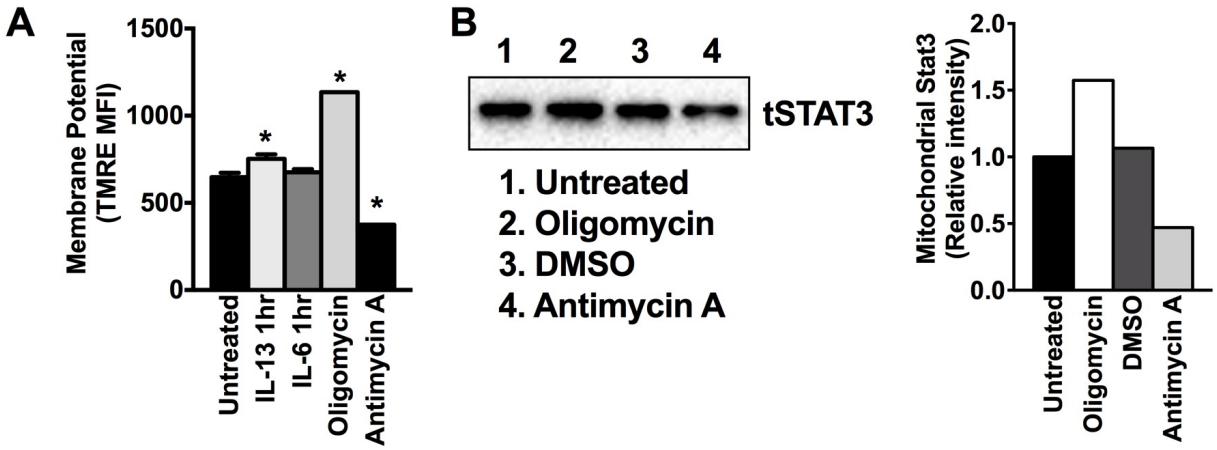

Figure 4.4. Mitochondrial Stat3 abundance is regulated by mitochondrial membrane potential. (A) Mitochondrial membrane potential as measured by TMRE staining in C2C12 myoblasts treated with rIl-13, rIl-6, Oligomycin or Antimycin A and measured by flow cytometry for mean fluorescence intensity. (B) Stat3 abundance in isolated mitochondria of C2C12 myotubes treated with Oligomycin, Antimycin A or DMSO control as measured by western blot in left panel and quantified in right panel. Data presented as mean ± SEM. *$p<0.05$.

Il-13 signaling in protein translation

Our transcriptional analysis revealed that Il-13 regulates a large program of mitochondrial and oxidative metabolic genes in skeletal muscle. Interestingly, the relative change in mitochondrial protein and functional output were greater than those of transcripts. This is consistent with a recent report showing that protein translation is enhanced by exercise training [76]. Of note, nuclear encoded mitochondrial transcripts are among the mRNAs with the longest half-life, potentially indicating the importance of post-transcriptional regulation [81]. Analysis of our RNA-seq data showed that the ribosome was also a major transcriptional target of Il-13 signaling in skeletal muscle. This observation led us to investigate whether Il-13 modulates translational activity in skeletal muscle.

Ribosomal RNA comprises the majority of total cell RNA content. We examined whether total RNA content was increased by Il-13. rIl-13 treatment increased total RNA content in C2C12 myotubes compared to protein content (Fig 4.5A). Polysome analysis was performed with the same amount of total RNA (1mg) followed by fractionation. The separation of ribosomes and polysomes based on density is indicative of the relative translational output. rIl-13 treatment reduced the abundance of monomeric ribosome components (40S, 60S, 80s), but increased polysome abundance (Fig 4.5B). RNA was isolated from the total input and polysome fractions to examine translation of individual transcripts. Polysomal 36B4, TATA-binding protein (TBP) and mitochondrial encoded ND1 did not change after IL-13 treatment. In contrast, there was an increase in the nuclear encoded mitochondrial genes Atp5s1, Ndufa6 and Mrps12 (Fig 4.5C). This

indicated that Il-13 promotes selective enrichment of mitochondrial transcripts in translationally active polysomes.

Next, we used metabolic labeling by ^{35}S-methionine to trace protein synthesis in C2C12 myotubes. rIl-13 did not significantly alter total protein translation determined by ^{35}S-methionine incorporation (Fig 4.5D). rIl-13 increased incorporation of ^{35}S into mitochondrial and cytosolic proteins but not nuclear proteins (Fig 4.5E). Lastly, we used control and Stat3$^{-/-}$ myotubes to examine whether Stat3 is required for Il-13 mediated changes in translational activity. Control myotubes showed a shift in polysome profile after rIl-13 treatment, which was abolished in myotubes lacking Stat3 (Fig 4.5F).

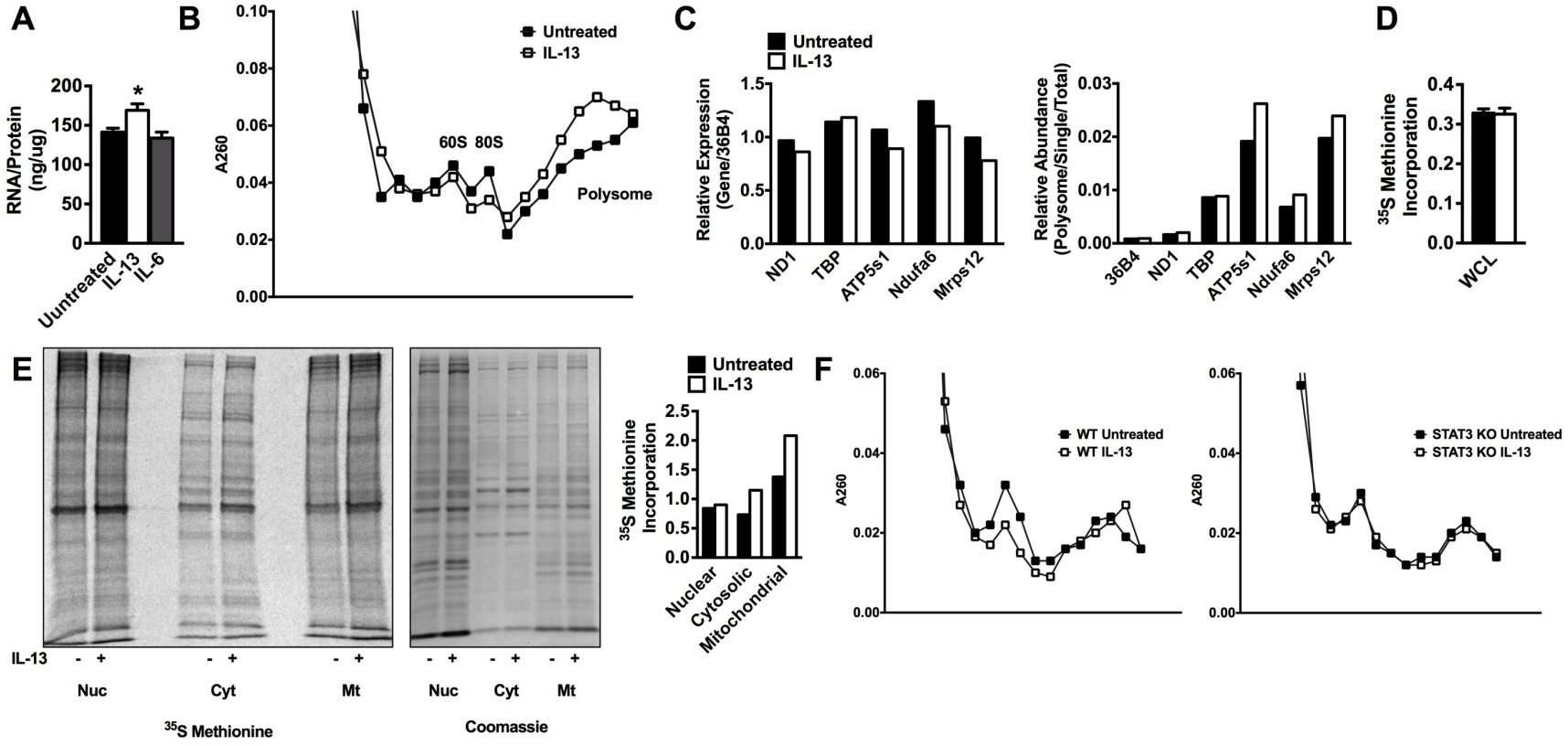
A
RNA/Protein (ng/ug)
200
150
100
50
0
*
Uuntreated
IL-13
IL-6
B
A260
0.10
0.08
0.06
0.04
0.02
0.00
Untreated
IL-13
60S 80S
Polysome
C
Untreated
IL-13
Relative Expression (Gene/36B4)
1.5
1.0
0.5
0.0
ND1
TBP
ATP5s1
Ndufa6
Mrps12
Relative Abundance (Polysome/Single/Total)
0.03
0.02
0.01
0.00
36B4
ND1
TBP
ATP5s1
Ndufa6
Mrps12
D
35S Methionine Incorporation
0.4
0.3
0.2
0.1
0.0
WCL
E
IL-13 - + - + - + - + - + - +
Nuc
Cyt
Mt
Nuc
Cyt
Mt
35S Methionine
Coomassie
Untreated
IL-13
35S Methionine Incorporation
2.5
2.0
1.5
1.0
0.5
0.0
Nuclear
Cytosolic
Mitochondrial
F
A260
0.06
0.04
0.02
0.00
WT Untreated
WT IL-13
STAT3 KO Untreated
STAT3 KO IL-13

Figure 4.5. Il-13 increases translation of mitochondrial proteins in C2C12 myotubes. (A) Total RNA content of C2C12 myotubes treated with rIl-13 and rIl-6 overnight normalized to protein content. (B) Polysome profiles of untreated and rIl-13 treated C2C12 myotubes treated for 6 hours. (C) Left panel: Relative expression of various genes normalized to 36B4 in total cell RNA from C2C12 myotubes treated with rIl-13 for 6 hours. Right panel: Expression of various genes in RNA isolated from polysome containing fractions in B. (D) Quantification of total ^{35}S methionine incorporation in C2C12 myotubes treated with rIl-13 for 6 hours. (E) ^{35}S methionine incorporation into nuclear (Nuc), cytosolic (Cyt) and mitochondrial (Mt) fractions of C2C12 myotubes treated with rIl-13 for 6 hours. Coomassie staining shown as loading control in middle panel and quantification shown on right. (F) Polysome profiles of untreated and rIl-13 treated WT and Stat3$^{-/-}$ C2C12 myotubes treated for 6 hours. Data presented as mean ± SEM. *$p<0.05$.

Discussion

Data presented above underscore the complex role of Stat3 downstream of Il-13 in skeletal muscle oxidative metabolism. We propose a model where Stat3 regulates mitochondrial respiration through multiple mechanisms to maximize muscle metabolic adaptation (Fig 4.6). Upon binding its heterodimeric receptor of Il-13Rα1 and Il-4R, Il-13 activates Jak kinases to phosphorylate Stat3 at tyrosine 705. Tyrosine phosphorylation drives Stat3 import to the nucleus where it binds regulatory elements and activates transcription of genes encoding Errα/γ, fatty acid oxidation, and mitochondrial oxidative metabolism. As a second tier of regulation, Il-13 activates ribosome biogenesis and translation of mitochondrial OxPhos genes. Lastly, Il-13 increases mitochondrial membrane potential and Stat3 import into mitochondria where it interacts directly with components of the electron transport chain including respiratory supercomplexes to enhance respiration. These three mechanisms collectively promote mitochondrial biogenesis and increase aerobic metabolism in exercise trained muscle.

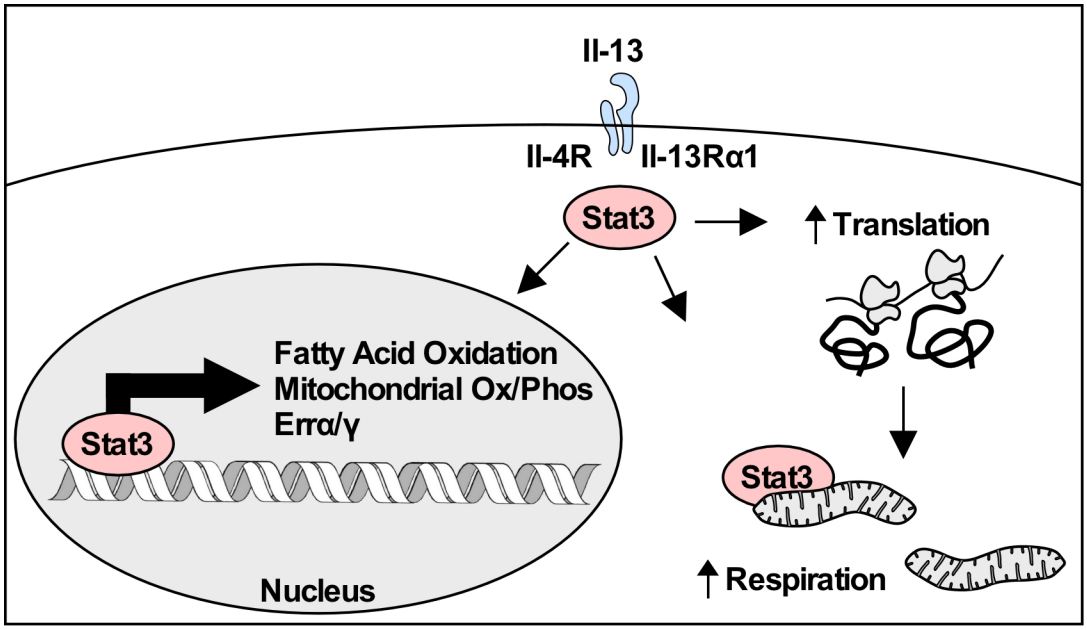

Figure 4.6. Il-13 signaling promotes mitochondrial oxidative metabolism through multiple levels of regulation. Il-13 increases tyrosine phosphorylation of Stat3 and nuclear translocation to increase transcription of fatty acid oxidation, mitochondrial OxPhos and Errα/γ genes. Il-13 may also increase the abundance of mitochondrial Stat3 and activate translation of mitochondrial proteins to drive mitochondrial respiration and biogenesis.

Final remarks

The immune system fine-tunes the homeostatic state of tissue in response to environmental and physiological stimuli. The hygiene hypothesis proposes that coevolution of humans and certain parasites has helped shaping the immune phenotype. This interaction may also play a role in modulation of metabolic fitness of the human hosts. For example, infection with helminth worm is predictive of higher maximal oxygen consumption or VO_2Max, a measure closely associated with endurance capacity [53]. Women infected with giant roundworm (Ascaris lumbricoides) have higher fertility compared to uninfected women [82]. In contrast, hookworm infection, which activates the classical Type 1 immune profile, reduced fertility [82]. Results from the current study, together with published work from others, suggest an intriguing link between helminth worm-induced type 2 immunity and metabolic adaptation capacity of muscle and adipose tissues. Future investigation into uncovering the molecular details of the beneficial host-parasite interaction may identify pathways to harness immune and metabolic responses that are dysregulated in disease conditions.

References

1. United States. Department of Health and Human Services., *2008 physical activity guidelines for Americans : be active, healthy, and happy!* ODPHP publication. 2008, Washington, DC: U.S. Dept. of Health and Human Services. ix, 61 p.

2. Li, Y., et al., *Impact of Healthy Lifestyle Factors on Life Expectancies in the US Population.* Circulation, 2018.

3. Hawley, J.A., et al., *Integrative biology of exercise.* Cell, 2014. **159**(4): p. 738-49.

4. Overmyer, K.A., et al., *Maximal oxidative capacity during exercise is associated with skeletal muscle fuel selection and dynamic changes in mitochondrial protein acetylation.* Cell Metab, 2015. **21**(3): p. 468-78.

5. Egan, B. and J.R. Zierath, *Exercise metabolism and the molecular regulation of skeletal muscle adaptation.* Cell Metab, 2013. **17**(2): p. 162-84.

6. LeBrasseur, N.K., K. Walsh, and Z. Arany, *Metabolic benefits of resistance training and fast glycolytic skeletal muscle.* Am J Physiol Endocrinol Metab, 2011. **300**(1): p. E3-10.

7. Holloszy, J.O., *Biochemical adaptations in muscle. Effects of exercise on mitochondrial oxygen uptake and respiratory enzyme activity in skeletal muscle.* J Biol Chem, 1967. **242**(9): p. 2278-82.

8. Wang, Y.X., et al., *Regulation of muscle fiber type and running endurance by PPARdelta.* PLoS Biol, 2004. **2**(10): p. e294.

9. Lin, J., et al., *Transcriptional co-activator PGC-1 alpha drives the formation of slow-twitch muscle fibres.* Nature, 2002. **418**(6899): p. 797-801.

10. Narkar, V.A., et al., *Exercise and PGC-1alpha-independent synchronization of type I muscle metabolism and vasculature by ERRgamma.* Cell Metab, 2011. **13**(3): p. 283-93.

11. Huss, J.M., et al., *Estrogen-related receptor alpha directs peroxisome proliferator-activated receptor alpha signaling in the transcriptional control of energy metabolism in cardiac and skeletal muscle.* Mol Cell Biol, 2004. **24**(20): p. 9079-91.

12. Reilly, S.M., et al., *Nuclear receptor corepressor SMRT regulates mitochondrial oxidative metabolism and mediates aging-related metabolic deterioration.* Cell Metab, 2010. **12**(6): p. 643-53.

13. Yamamoto, H., et al., *NCoR1 is a conserved physiological modulator of muscle mass and oxidative function.* Cell, 2011. **147**(4): p. 827-39.

14. Calvo, J.A., et al., *Muscle-specific expression of PPARgamma coactivator-1alpha improves exercise performance and increases peak oxygen uptake.* J Appl Physiol (1985), 2008. **104**(5): p. 1304-12.

15. Narkar, V.A., et al., *AMPK and PPARdelta agonists are exercise mimetics.* Cell, 2008. **134**(3): p. 405-15.

16. Fan, W., et al., *PPARdelta Promotes Running Endurance by Preserving Glucose.* Cell Metab, 2017. **25**(5): p. 1186-1193 e4.

17. Medzhitov, R., *Origin and physiological roles of inflammation.* Nature, 2008. **454**(7203): p. 428-35.

18. Hotamisligil, G.S., *Inflammation and metabolic disorders.* Nature, 2006. **444**(7121): p. 860-7.

19. Nishimura, S., et al., *CD8+ effector T cells contribute to macrophage recruitment and adipose tissue inflammation in obesity.* Nat Med, 2009. **15**(8): p. 914-20.

20. Yang, H., et al., *Obesity increases the production of proinflammatory mediators from adipose tissue T cells and compromises TCR repertoire diversity: implications for systemic inflammation and insulin resistance.* J Immunol, 2010. **185**(3): p. 1836-45.

21. Liu, J., et al., *Genetic deficiency and pharmacological stabilization of mast cells reduce diet-induced obesity and diabetes in mice.* Nat Med, 2009. **15**(8): p. 940-5.

22. Feuerer, M., et al., *Lean, but not obese, fat is enriched for a unique population of regulatory T cells that affect metabolic parameters.* Nat Med, 2009. **15**(8): p. 930-9.

23. Ji, Y., et al., *Activation of natural killer T cells promotes M2 Macrophage polarization in adipose tissue and improves systemic glucose tolerance via interleukin-4 (IL-4)/STAT6 protein signaling axis in obesity.* J Biol Chem, 2012. **287**(17): p. 13561-71.

24. Lynch, L., et al., *Adipose tissue invariant NKT cells protect against diet-induced obesity and metabolic disorder through regulatory cytokine production.* Immunity, 2012. **37**(3): p. 574-87.

25. Knudsen, N.H. and C.H. Lee, *Identity Crisis: CD301b(+) Mononuclear Phagocytes Blur the M1-M2 Macrophage Line.* Immunity, 2016. **45**(3): p. 461-3.

26. Odegaard, J.I. and A. Chawla, *Pleiotropic actions of insulin resistance and inflammation in metabolic homeostasis.* Science, 2013. **339**(6116): p. 172-7.

27. Pulendran, B. and D. Artis, *New paradigms in type 2 immunity.* Science, 2012. **337**(6093): p. 431-5.

28. Kang, K., et al., *Adipocyte-derived Th2 cytokines and myeloid PPARdelta regulate macrophage polarization and insulin sensitivity.* Cell Metab, 2008. **7**(6): p. 485-95.

29. Odegaard, J.I., et al., *Macrophage-specific PPARgamma controls alternative activation and improves insulin resistance.* Nature, 2007. **447**(7148): p. 1116-20.

30. Heredia, J.E., et al., *Type 2 innate signals stimulate fibro/adipogenic progenitors to facilitate muscle regeneration.* Cell, 2013. **153**(2): p. 376-88.

31. Stanya, K.J., et al., *Direct control of hepatic glucose production by interleukin-13 in mice.* J Clin Invest, 2013. **123**(1): p. 261-71.

32. Orchansky, P.L., et al., *Characterization of the cytoplasmic domain of interleukin-13 receptor-alpha.* J Biol Chem, 1999. **274**(30): p. 20818-25.

33. Neill, D.R., et al., *Nuocytes represent a new innate effector leukocyte that mediates type-2 immunity.* Nature, 2010. **464**(7293): p. 1367-70.

34. Moro, K., et al., *Innate production of T(H)2 cytokines by adipose tissue-associated c-Kit(+)Sca-1(+) lymphoid cells.* Nature, 2010. **463**(7280): p. 540-4.

35. Price, A.E., et al., *Systemically dispersed innate IL-13-expressing cells in type 2 immunity.* Proc Natl Acad Sci U S A, 2010. **107**(25): p. 11489-94.

36. Brestoff, J.R., et al., *Group 2 innate lymphoid cells promote beiging of white adipose tissue and limit obesity.* Nature, 2015. **519**(7542): p. 242-6.

37. Lee, M.W., et al., *Activated type 2 innate lymphoid cells regulate beige fat biogenesis.* Cell, 2015. **160**(1-2): p. 74-87.

38. Nguyen, K.D., et al., *Alternatively activated macrophages produce catecholamines to sustain adaptive thermogenesis.* Nature, 2011. **480**(7375): p. 104-8.

39. Qiu, Y., et al., *Eosinophils and type 2 cytokine signaling in macrophages orchestrate development of functional beige fat.* Cell, 2014. **157**(6): p. 1292-308.

40. Rao, R.R., et al., *Meteorin-like is a hormone that regulates immune-adipose interactions to increase beige fat thermogenesis.* Cell, 2014. **157**(6): p. 1279-91.

41. Fischer, K., et al., *Alternatively activated macrophages do not synthesize catecholamines or contribute to adipose tissue adaptive thermogenesis.* Nat Med, 2017. **23**(5): p. 623-630.

42. Wu, M.V., et al., *Thermogenic capacity is antagonistically regulated in classical brown and white subcutaneous fat depots by high fat diet and endurance training in rats: impact on whole-body energy expenditure.* J Biol Chem, 2014. **289**(49): p. 34129-40.

43. Goldstein, M.S., *Humoral nature of the hypoglycemic factor of muscular work.* Diabetes, 1961. **10**: p. 232-4.

44. Pedersen, B.K. and M.A. Febbraio, *Muscles, exercise and obesity: skeletal muscle as a secretory organ.* Nat Rev Endocrinol, 2012. **8**(8): p. 457-65.

45. Di Gregorio, G.B., et al., *Lipid and carbohydrate metabolism in mice with a targeted mutation in the IL-6 gene: absence of development of age-related obesity.* Am J Physiol Endocrinol Metab, 2004. **287**(1): p. E182-7.

46. O'Neill, H.M., et al., *IL-6 is not essential for exercise-induced increases in glucose uptake.* J Appl Physiol (1985), 2013. **114**(9): p. 1151-7.

47. Fueger, P.T., et al., *Control of exercise-stimulated muscle glucose uptake by GLUT4 is dependent on glucose phosphorylation capacity in the conscious mouse.* J Biol Chem, 2004. **279**(49): p. 50956-61.

48. Romijn, J.A., et al., *Regulation of endogenous fat and carbohydrate metabolism in relation to exercise intensity and duration.* Am J Physiol, 1993. **265**(3 Pt 1): p. E380-91.

49. Rangwala, S.M., et al., *Estrogen-related receptor gamma is a key regulator of muscle mitochondrial activity and oxidative capacity.* J Biol Chem, 2010. **285**(29): p. 22619-29.

50. Wang, T., et al., *Estrogen-related receptor alpha (ERRalpha) and ERRgamma are essential coordinators of cardiac metabolism and function.* Mol Cell Biol, 2015. **35**(7): p. 1281-98.

51. Dufour, C.R., et al., *Genome-wide orchestration of cardiac functions by the orphan nuclear receptors ERRalpha and gamma.* Cell Metab, 2007. **5**(5): p. 345-56.

52. Audet-Walsh, E. and V. Giguere, *The multiple universes of estrogen-related receptor alpha and gamma in metabolic control and related diseases.* Acta Pharmacol Sin, 2015. **36**(1): p. 51-61.

53. Pisor, A.C., et al., *Patterns of senescence in human cardiovascular fitness: VO2 max in subsistence and industrialized populations.* Am J Hum Biol, 2013. **25**(6): p. 756-69.

54. Takeda, K., et al., *Stat3 activation is responsible for IL-6-dependent T cell proliferation through preventing apoptosis: generation and characterization of T cell-specific Stat3-deficient mice.* J Immunol, 1998. **161**(9): p. 4652-60.

55. Shalem, O., et al., *Genome-scale CRISPR-Cas9 knockout screening in human cells.* Science, 2014. **343**(6166): p. 84-87.

56. Sanjana, N.E., O. Shalem, and F. Zhang, *Improved vectors and genome-wide libraries for CRISPR screening.* Nat Methods, 2014. **11**(8): p. 783-784.

57. Gruntman, A.M., et al., *Gene transfer in skeletal and cardiac muscle using recombinant adeno-associated virus.* Curr Protoc Microbiol, 2013. **Chapter 14**: p. Unit 14D 3.

58. Boutagy, N.E., et al., *Isolation of Mitochondria from Minimal Quantities of Mouse Skeletal Muscle for High Throughput Microplate Respiratory Measurements.* J Vis Exp, 2015(105).

59. Jacobi, D., et al., *Hepatic Bmal1 Regulates Rhythmic Mitochondrial Dynamics and Promotes Metabolic Fitness.* Cell Metab, 2015. **22**(4): p. 709-20.

60. Sidossis, L. and S. Kajimura, *Brown and beige fat in humans: thermogenic adipocytes that control energy and glucose homeostasis.* J Clin Invest, 2015. **125**(2): p. 478-86.

61. Harms, M. and P. Seale, *Brown and beige fat: development, function and therapeutic potential.* Nat Med, 2013. **19**(10): p. 1252-63.

62. Puigserver, P., et al., *A cold-inducible coactivator of nuclear receptors linked to adaptive thermogenesis.* Cell, 1998. **92**(6): p. 829-39.

63. Villena, J.A., et al., *Orphan nuclear receptor estrogen-related receptor alpha is essential for adaptive thermogenesis.* Proc Natl Acad Sci U S A, 2007. **104**(4): p. 1418-23.

64. Ahmadian, M., et al., *ERRgamma Preserves Brown Fat Innate Thermogenic Activity.* Cell Rep, 2018. **22**(11): p. 2849-2859.

65. Hepler, C., L. Vishvanath, and R.K. Gupta, *Sorting out adipocyte precursors and their role in physiology and disease.* Genes Dev, 2017. **31**(2): p. 127-140.

66. Stanford, K.I., R.J. Middelbeek, and L.J. Goodyear, *Exercise Effects on White Adipose Tissue: Beiging and Metabolic Adaptations.* Diabetes, 2015. **64**(7): p. 2361-8.

67. Boström, P., et al., *A PGC1-α-dependent myokine that drives brown-fat-like development of white fat and thermogenesis.* Nature, 2012. **481**(7382): p. 463-8.

68. Loyd, C., et al., *Fibroblast growth factor 21 is required for beneficial effects of exercise during chronic high-fat feeding.* J Appl Physiol (1985), 2016. **121**(3): p. 687-98.

69. Fisher, F.M., et al., *FGF21 regulates PGC-1alpha and browning of white adipose tissues in adaptive thermogenesis.* Genes Dev, 2012. **26**(3): p. 271-81.

70. Bordicchia, M., et al., *Cardiac natriuretic peptides act via p38 MAPK to induce the brown fat thermogenic program in mouse and human adipocytes.* J Clin Invest, 2012. **122**(3): p. 1022-36.

71. Cardoso, V., et al., *Neuronal regulation of type 2 innate lymphoid cells via neuromedin U.* Nature, 2017. **549**(7671): p. 277-281.

72. Klose, C.S.N., et al., *The neuropeptide neuromedin U stimulates innate lymphoid cells and type 2 inflammation.* Nature, 2017. **549**(7671): p. 282-286.

73. Wallrapp, A., et al., *The neuropeptide NMU amplifies ILC2-driven allergic lung inflammation.* Nature, 2017. **549**(7672): p. 351-356.

74. Fontaine, D.A. and D.B. Davis, *Attention to Background Strain Is Essential for Metabolic Research: C57BL/6 and the International Knockout Mouse Consortium.* Diabetes, 2016. **65**(1): p. 25-33.

75. Vats, D., et al., *Oxidative metabolism and PGC-1beta attenuate macrophage-mediated inflammation.* Cell Metab, 2006. **4**(1): p. 13-24.

76. Robinson, M.M., et al., *Enhanced Protein Translation Underlies Improved Metabolic and Physical Adaptations to Different Exercise Training Modes in Young and Old Humans.* Cell Metab, 2017. **25**(3): p. 581-592.

77. Greggio, C., et al., *Enhanced Respiratory Chain Supercomplex Formation in Response to Exercise in Human Skeletal Muscle.* Cell Metab, 2017. **25**(2): p. 301-311.

78. Wegrzyn, J., et al., *Function of mitochondrial Stat3 in cellular respiration.* Science, 2009. **323**(5915): p. 793-7.

79. Szczepanek, K., et al., *Mitochondrial-targeted Signal transducer and activator of transcription 3 (STAT3) protects against ischemia-induced changes in the electron transport chain and the generation of reactive oxygen species.* J Biol Chem, 2011. **286**(34): p. 29610-20.

80. Gough, D.J., et al., *Mitochondrial STAT3 supports Ras-dependent oncogenic transformation.* Science, 2009. **324**(5935): p. 1713-6.

81. Jovanovic, M., et al., *Immunogenetics. Dynamic profiling of the protein life cycle in response to pathogens.* Science, 2015. **347**(6226): p. 1259038.

82. Blackwell, A.D., et al., *Helminth infection, fecundity, and age of first pregnancy in women.* Science, 2015. **350**(6263): p. 970-2.